A deep scattering layer under the North Pole pack ice

Progress in Oceanography 194 (2021) 102560

Contents lists available at ScienceDirect

Progress in Oceanography

journal homepage: www.elsevier.com/locate/pocean

A deep scattering layer under the North Pole pack ice

Pauline Snoeijs-Leijonmalm [a,*], Harald Gjøsæter [b], Randi B. Ingvaldsen [b], Tor Knutsen [b], Rolf Korneliussen [b], Egil Ona [b], Hein Rune Skjoldal [b], Christian Stranne [c], Larry Mayer [d], Martin Jakobsson [c], Katarina Gårdfeldt [e]

[a] Department of Ecology, Environment and Plant Sciences, Stockholm University, SE-10691 Stockholm, Sweden
[b] Institute of Marine Research, Nordnesgaten 50, NO-5005 Bergen, Norway
[c] Department of Geological Sciences, Stockholm University, SE-10691 Stockholm, Sweden
[d] Center for Coastal and Ocean Mapping, University of New Hampshire, Durham, NH, USA
[e] Department for Chemistry and Chemical Engineering, Chalmers University of Technology, Gothenburg, Sweden

ARTICLE INFO

Keywords:
Acoustics
Arctogadus
Atlantic water layer
Boreogadus
Central Arctic Ocean (CAO)
Echosounder
Siphonophore

ABSTRACT

The 3.3 million km^2 marine ecosystem around the North Pole, defined as the Central Arctic Ocean (CAO), is a blind spot on the map of the world's fish stocks. The CAO essentially comprises the permanently ice-covered deep basins and ridges outside the continental shelves, and is only accessible by ice-breakers. Traditional trawling for assessing fish stocks is impossible under the thick pack ice, and coherent hydroacoustic surveys are unachievable due to ice-breaking noise. Consequently, nothing is known about the existence of any pelagic fish stocks in the CAO, although juveniles of *Boreogadus saida* richly occur at the surface associated with the sea ice and ice-associated *Arctogadus glacialis* has been reported as well. We here present a first indication of a possible mesopelagic fish stock in the CAO. We had the opportunity to analyse a geophysical hydroacoustic data set with 13 time windows of usable acoustic data over a transect from 84.4 °N in the Nansen Basin, across the North Pole (90.0 °N), to 82.4 °N in the Canada Basin. We discovered a deep scattering layer (DSL), suggesting the presence of zooplankton and fish, at 300–600 m of depth in the Atlantic water layer of the CAO. Maximum possible fish abundance and biomass was very low; values of ca. 2,000 individuals km^{-2} and ca. 50 kg km^{-2} were calculated for the DSL in the North-Pole area according to a model assuming that all acoustic backscatter represents 15-cm long *B. saida* and/or *A. glacialis*. The true abundance and biomass of fish is even lower than this, but cannot be quantified from this dataset due to possible backscatter originating from pneumatophores of physonect siphonophores that are known to occur in the area. Further studies on the DSL of the CAO should include sampling and identification of the backscattering organisms. From our study we can conclude that if the central Arctic DSL contains fish, their biomass is currently too low for any sustainable fishery.

1. Introduction

The "Central Arctic Ocean" (CAO) is defined as the permanently ice-covered deep basins and ridges outside the continental shelves of the Arctic Ocean (Fig. 1; PAME, 2013). For the CAO Large Marine Ecosystem (LME), there is an almost complete absence of knowledge of the occurrence of pelagic fish as a key ecological link between zooplankton and seals, whales and polar bears (Van Pelt et al., 2017). The reason for the absence of data from the CAO LME is related to the difficulty of accessing this remote cold area for on-site research due to its 2–3 m thick year-round sea-ice cover. Traditional trawling for assessing fish stocks is impossible under the pack ice. The area is only accessible by icebreakers, and acoustic data targeting the water column cannot be used if acquired while ice-breaking due to the high noise level. The fish stocks of the (partly) seasonally ice-covered Arctic shelf seas are relatively unknown as well, apart from those of the well-investigated, monitored and managed Barents Sea (Hansen et al., 2019; ICES, 2019a,b).

The CAO LME is changing rapidly as a result of global climate change. Large ecosystem transformations are likely happening with the loss of the sea ice, even before the baselines of its ecological communities are properly known and marine assessment and conservation measures are in place (Christiansen et al., 2014; Bluhm et al., 2015; Harris et al., 2018). The CAO is becoming a more dynamic ecosystem with global warming, as the marginal ice zone moves further north in

* Corresponding author.
E-mail address: pauline.snoeijs-leijonmalm@su.se (P. Snoeijs-Leijonmalm).

https://doi.org/10.1016/j.pocean.2021.102560
Received 25 June 2020; Received in revised form 27 January 2021; Accepted 11 March 2021
Available online 19 March 2021

summer and south again in winter (Overland and Wang, 2013). The extent of both the Arctic summer and winter minimum sea-ice cover has consistently been breaking negative records during the past decades: the minimum summer Arctic sea ice extent has decreased with an estimated loss rate of ca. 1 million km^2 (ca. 13.2%) per decade between 1979 and 2017 (IPCC, 2013, 2018; Barnhart et al., 2015; Ding et al., 2017). Simultaneously, the sea ice is also thinning (Laxon et al., 2013, Kwok, 2018), with an estimated loss rate of ca. 3,100 km^3 (ca. 13.5%) per decade over the period 1979–2017. Climate models for the Arctic region predict a further decline of the summer sea-ice cover to below 1 million km^2 within the coming 30 years, depending on which political decisions are made and implemented at a global scale (Duarte et al., 2012; Screen and Williamson, 2017).

The rapid environmental changes in the CAO LME create new circumstances that may impact ecological and social values, including future commercial fisheries (Christiansen et al., 2014). A large part of the CAO is "High Seas" area (Fig. S1), i.e., international waters beyond the Exclusive Economic Zones (EEZs) of the Arctic coastal states, where all states have rights and obligations according to the United Nations Convention on the Law of the Sea (UNCLOS, 1982). Lessons learnt from other marine LMEs worldwide are that (1) exploitation of newly accessible natural resources tends to precede scientific research and effective management measures, and (2) internationally shared fish stocks in High Seas are especially prone to overexploitation (McWhinnie, 2009). Recognising that, apart from a few anecdotal reports (e.g., single unidentified fish observed from submarine windows), nothing is known about the existence of any pelagic fish stocks (FiSCAO, 2017, 2018), a precautionary approach has recently been taken for the CAO before any exploitation of its potential fishery resources. In November 2018, politicians from nine nations (including the five coastal states) and the EU decided to put "science first" and not to engage in commercial fishing for 16 years after the *Agreement to Prevent Unregulated High Seas Fisheries in the CAO* (Hoag, 2017; EU, 2019) has entered into force. This Agreement also includes the installation of a Joint Program of Scientific Research and Monitoring for the CAO. To date, the agreement has been ratified by nine of the ten Signatories. Commercial fishing does

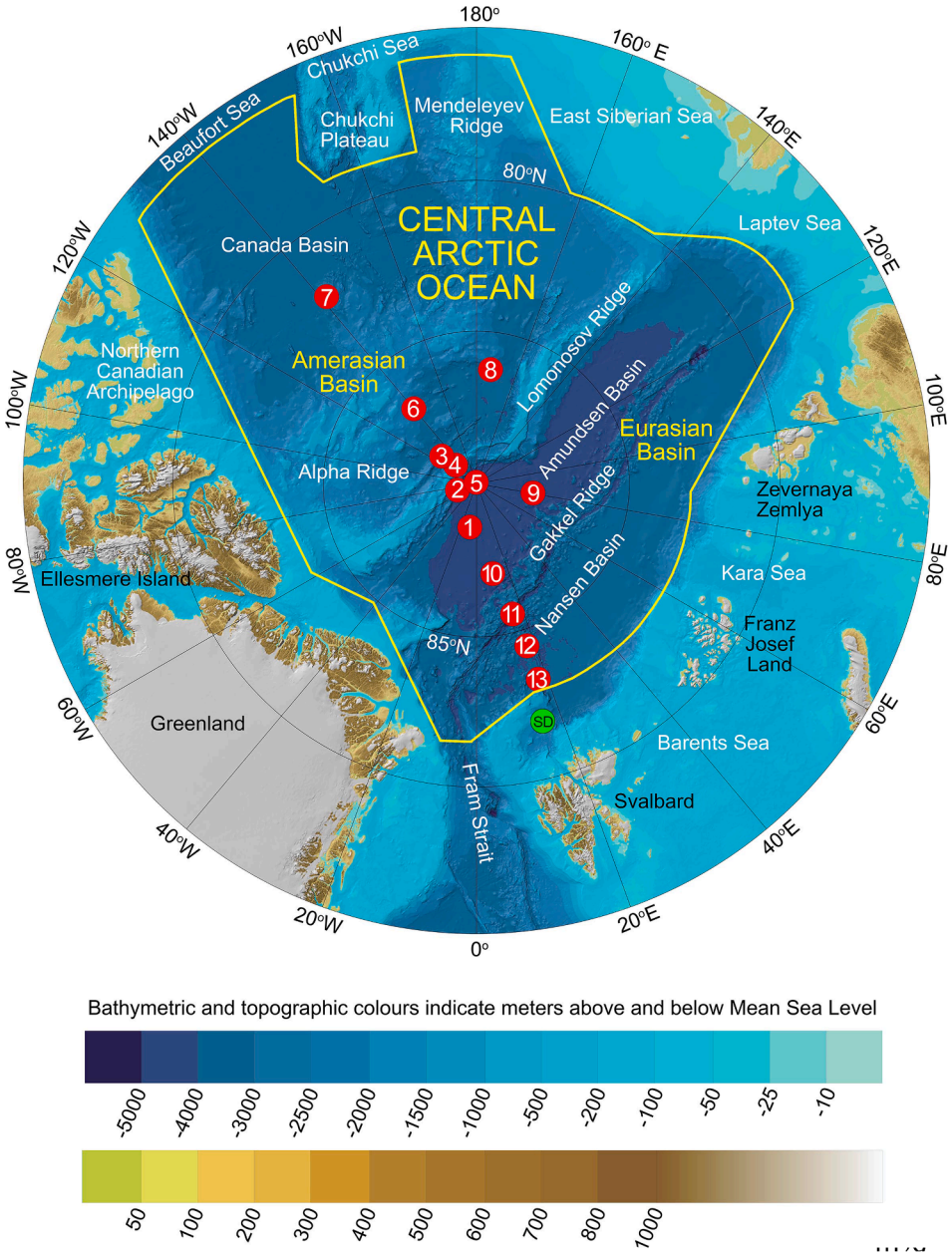

Fig. 1. Map of the Central Arctic Ocean (CAO), showing the positions of the acoustic sampling stations (Stations 1–13) visited during the "Arctic Ocean 2016" expedition with *IB Oden* between 15 August and 15 September 2016. The stations were located along a transect between 83.2 °N in the Nansen Basin, across the Amundsen Basin, the North Pole, the Lomonosov Ridge, and ending in the Canada Basin at 82.4 °N. Each of the stations represents a time window during the expedition when the icebreaker was drifting with the sea ice at <1 knot, i.e., not causing excessive noise from breaking ice. Apart from Station 4 at the Lomonosov Ridge (1,244 m), the water depth at all stations was >2,000 m with maximum depth at Station 11 in the valley along the Gakkel Ridge (4,952 m). SD = the Sofia Deep, the hitherto northernmost reported mesopelagic scattering layer at 82.10 °N (Gjøsæter et al., 2017). The background map was extracted from the International Bathymetric Chart of the Arctic Ocean (IBCAO), Version 3.0 (Jakobsson et al., 2012). Physiographic classifications of the CAO and the High Seas (the area outside national Exclusive Economic Zones) of the Arctic Ocean are shown in Fig. S1.

not occur in the CAO today because the yearly ice-free time window is still only local and short (some weeks). Furthermore, no resources of potential commercial value have so far been detected (FiSCAO, 2017, 2018; Snoeijs-Leijonmalm et al., 2020).

In this paper we present a first indication of what could be mesopelagic fish under the pack-ice cover of the CAO. We discovered a consistent deep scattering layer (DSL), i.e., a horizontal zone with living organisms (zooplankton and fish) detected as acoustic backscatter by an echosounder. The DSL was detected in the Atlantic water layer at 300–600 m of depth with highest density around the North Pole. DSLs are a near universal feature throughout the world's oceans at depths of 200–1,000 m (Irigoien et al., 2014; Klevjer et al., 2016). A mesopelagic DSL occurs across the entire Fram Strait at the Atlantic entrance to the Arctic Ocean (Gjøsæter et al., 2020; Fig. 1), but whether a DSL would occur in the CAO outside the continental shelves remained an open question. We were able to perform the present study through access to data collected under the pack ice of the CAO during the "Arctic Ocean 2016" expedition with the Swedish ice-breaker (*IB*) *Oden* (Gårdfeldt and Lindgren, 2016). Acoustic and oceanographic data were collected along a transect from 84.4 °N in the Nansen Basin across the Amundsen Basin, the North Pole (90.0 °N), and the Lomonosov Ridge to the Canada Basin at 82.4 °N.

2. Material and methods

2.1. Area description

The boundaries of the CAO LME basically follow the shelf edge, as defined by the Arctic Council (PAME, 2013; Fig. 1), but in the Canadian Basin, the boundary between the CAO and Beaufort Sea is along 76 °N, leaving the deep southern portion of the basin as part of the Beaufort Sea LME. The CAO is the largest of the Arctic LMEs with an area of ca. 3.3 million km^2, and essentially comprises the deep basins of the Arctic Ocean as well as ridges and sea mounts within the area (Fig. S1a). The most prominent feature of the CAO is the drifting sea ice that covers more or less the whole area during both winter and summer. However, the multi-year pack ice is disappearing fast and is being replaced by seasonal sea ice (Kwok, 2018).

The part of the Arctic Ocean that is most vulnerable to possible future exploitation of fishery resources is the ca. 2.8 million km^2 High Seas area outside the EEZs (Fig. S1b). The High Seas area overlaps to a large extent with the CAO, but includes also smaller portions of continental slopes and shelf regions, most notably the Chukchi Plateau (Fig. 1). The CAO and the High Seas contain about equal proportions of ridges (40–43%) and abyssal plains (33–34%) whereas the CAO contains more continental rises (22% compared to 15% for the High Seas) and the High Seas contains more continental shelf (3% compared to 0% for the CAO) (Fig. S1).

2.2. Acoustic sampling stations

Acoustic broadband backscatter data were collected from the water column between 15 August and 15 September 2016 during the "Arctic Ocean 2016" expedition with *IB Oden* (Gårdfeldt and Lindgren, 2016). The acoustic data grouped into 13 geographically separate areas with usable acoustic measurements corresponding to the geographical positions where station work (CTD and other) was conducted during the expedition (Fig. 1). Each of the stations represents a time window when the engines of the icebreaker were turned off and the ship was drifting with the Arctic transpolar ice drift (Spall, 2019) at <1 knot, i.e., not causing excessive noise from breaking ice. Apart from Station 4 at the Lomonosov Ridge (1,244 m), the water depth at all stations was >2,000 m with maximum depth at Station 11 in the valley along the Gakkel Ridge (4,952 m).

A comparison of the 13 areas showed that the minimum distance between them was 30 nmi (56 km) while the maximum distance within areas was 8 nmi (15 km). The midpoint of each area (average latitude and average longitude) is considered one sampling station (Table 1). The stations were labelled "Stations 1–13" along a transect starting at 83.2 °N in the Nansen Basin, across the Eurasian Basin (Nansen Basin, Gakkel Ridge, Amundsen Basin), the North Pole (90 °N), the Lomonosov Ridge, and ending in the Amerasian Basin (Alpha Ridge and Canada Basin) at 82.4 °N. All 13 stations fall within the CAO LME and 12 stations fall within the High Seas (the exception is Station 13 in the Norwegian EEZ) (Fig. S1).

2.3. Acoustic data collection and scrutinization

The acoustic data were originally collected for geophysical and oceanographic purposes to study double diffusive convection and vertical heat transport (Stranne et al., 2017) as well as mixed layer depth variability (Stranne et al., 2018), but we used them in the present paper as "data-of-opportunity" to detect living organisms. The data were not optimal due to the combination of high noise levels, acoustic backscatter measured over a single narrow frequency band, and low densities of organisms. However, after frequency selection, pulse compression and noise removal, the echograms were suitable for echo counting and confirming the existence of a DSL.

Acoustic backscatter was recorded from an echosounder (Simrad EK80) configured with a resonant (18 kHz) transducer (Simrad ES18-11) behind a 40-mm-thick polycarbonate plate ("window") mounted in the ice knife, aft of its cutting front. The echosounder pulse lengths were adjusted over a range of 1–8 ms with a linear up-sweep chirp from 15 to 30 kHz with fast up-ramping of the pulse, using 1.6% of the pulse duration for up-ramping. The transmit-power was set to 2000 W. It was synchronized with the on-board multibeam echosounder (12 kHz) and sub-bottom profiler (2.5–7 kHz) throughout the data collection period. The data were logged directly to large storage arrays in the Simrad raw format.

When inspecting the raw data, we found that the noise level within the echosounder band increased by 20–30 dB when the ship was steaming through and breaking ice, and for this reason the data could not be used. However, when the icebreaker was drifting with the sea ice at <1 knot, i.e., not causing excessive noise from breaking ice, the noise level was reduced to about −140 dB rel. 1 W in active mode (Simrad, 2018), and we were able to observe backscatter from individual living organisms in the water column. Based on these observations, a plot of the ship speed was used to select all the data with ship speed < 1 knot. Only these data were further processed and scrutinized.

The data selected on the basis of ship speed was pre-processed using the software LSSS (Large-Scale Survey System; Korneliussen et al., 2006, 2016) to remove noise and detect tracks, as well as to provide information that might be helpful when allocating backscatter to acoustic categories. Most of the remaining noise while the ship was drifting with the sea ice seemed to be electrical interference from the vessel's power system or other instruments. A typical signal-to-noise ratio of 10–12 dB could be achieved in the mesopelagic layer from 300 m down to 600 m depth. This mostly corresponded with the maximum depth of the observed backscattering of single targets. The data pre-processing (prior to scrutiny) proceeded as follows:

1. The nominal frequency was 18 kHz, but the original broadband data spanned over 15–30 kHz. The band 18 ± 2 kHz (16–20 kHz) was pulse-compressed and used in further processing because inspection of the data showed that background noise was at a minimum within this band (Fig. S2a).
2. The data were smoothed vertically with a Gaussian kernel of 0.5 m in diameter, i.e., the samples 0.25 m below and 0.25 m above were given half the weight of the sample centre during smoothing.
3. Spikes with duration longer than 1 ms were removed. In the slightly overlapping depth ranges 10–100 m, 90–250 m and 240–2400 m, spikes that were respectively 12 dB, 9 dB and 6 dB stronger than the

Table 1
Summary of data collection characteristics at Stations 1–13 visited during the "Arctic Ocean 2016" expedition with *IB Oden* between 15 August and 15 September 2016 (Fig. 1). The stations were located along a transect between 83.2 °N in the Nansen Basin, across the Amundsen Basin, the North Pole, the Lomonosov Ridge, and ending in the Canada Basin at 82.4 °N. Each of the stations represents a time window during the expedition when the icebreaker was drifting with the sea ice at < 1 knot, i.e., not causing excessive noise from breaking ice. The columns under "Acoustic data collection" show the date and time when the acoustic measurements started and ended, average latitude and longitude, station water depth, pulse length, gain, the number of acoustic profiles, and corrections for the area scattering coefficient (NASC) and the target strength (TS). The columns under "CTD data collection" show the date, time, latitude, longitude and water depth for the measurements of water temperature, salinity, density and oxygen concentration made at the same location as – or close by – the acoustic sampling stations. Note that the CTD data for Station 1 were measured with a time lag and that no CTD measurements were made at Station 4.

Station number	Acoustic data collection												CTD data collection				
	Start date	Start time (UTC)	End date	End time (UTC)	Average latitude (decimal)	Average longitude (decimal)	Average depth (m) ± STD	Pulse length (ms)	Gain	Acoustic profiles (number)	NASC Correction factor	TS detections (number)	TS correction (dB)	Date	Time (UTC)	Latitude (decimal)	Longitude (decimal)	Depth (m)
1	15 Aug	00:08	15 Aug	05:58	88.5013	−6.6283	4344 ± 7	8	18.5	48	Divided by 11.5	632	−5.3	11 Sep	10:58	88.0412	10.1066	4349
2	16 Aug	10:19	17 Aug	09:48	89.2657	−65.6178	3471 ± 545	8	18.5	193	Divided by 11.5	5240	−5.3	16 Aug	05:44	89.3398	−70.1707	3719
3	20 Aug	09:29	20 Aug	15:22	88.5311	−128.3094	3928 ± 31	8	18.5	65	Divided by 11.5	1095	−5.3	20 Aug	09:50	88.5374	−127.7919	3935
4	20 Aug	22:15	21 Aug	00:08	89.0795	−130.6097	1244 ± 7	8	18.5	22	Divided by 11.5	221	−5.3	No data	No data	No data	No data	No data
5	21 Aug	11:45	21 Aug	16:34	89.9740	65.0556	4211 ± 49	8	18.5	159	Divided by 11.5	6290	−5.3	21 Aug	13:57	89.9887	51.5042	4219
	21 Aug	16:35	21 Aug	16:39				4	18.4		−5.4							
	21 Aug	16:40	21 Aug	16:57				8	18.5		Divided by 12.0		−5.3					
	21 Aug	16:58	21 Aug	17:12				4	18.4		−5.4							
	21 Aug	17:13	21 Aug	17:27				2	17.8		Divided by 15.8		−6.0					
	21 Aug	17:28	21 Aug	23:03				8	18.5		Divided by 11.5		−5.3					
6	26 Aug	11:50	27 Aug	10:47	86.8294	−140.1930	2096 ± 424	8	18.5	355	Divided by 11.5	168	−5.3	26 Aug	09:19	86.7438	−140.9184	2703
	27 Aug	10:48	27 Aug	14:05				4	18.4		−5.4							
7	2 Sept	06:30	2 Sept	08:22	82.4028	−141.5803	2746 ± 82	4	18.4	151	Divided by 12.0	20	−5.4	2 Sept	07:02	82.3926	−141.7211	2692
	2 Sept	08:23	2 Sept	16:58				2	17.8		−6.0							
8	5 Sept	09:09	5 Sept	11:30	86.2113	172.7327	3900 ± 70	2	17.8	28	Divided by 15.8	0	−6.0	5 Sept	08:50	86.2027	172.7642	3832
9	9 Sept	23:52	10 Sept	03:16	88.0620	80.2991	4371 ± 22	2	17.8	51	Divided by 15.8	1	−6.0	9 Sept	23:30	88.0581	80.2630	4374
10	12 Sept	08:18	12 Sept	12:53	86.9965	10.4428	4328 ± 28	2	17.8	54	Divided by 15.8	0	−6.0	12 Sept	07:40	86.9902	10.3028	4324
11	13 Sept	10:59	13 Sept	19:54	85.5253	15.6403	4952 ± 36	2	17.8	87	Divided by 15.8	0	−6.0	13 Sept	10:48	85.5211	15.6435	4944
12	14 Sept	07:51	14 Sept	16:40	84.4056	17.4301	3804 ± 53	2	17.8	107	Divided by 15.8	0	−6.0	14 Sept	08:51	84.4055	17.3946	3841
13	15 Sept	07:52	15 Sept	11:08	83.2409	17.6704	4019 ± 2	2	17.8	43	Divided by 15.8	0	−6.0	15 Sept	08:48	83.2436	17.6628	4020

mean values of samples in the neighbouring pings were removed. The reason for requiring spikes to be stronger at short ranges is that the beam footprint is narrower at short ranges, i.e., small schools could more easily be detected by one ping at short ranges than at long ranges, and thereby be detected as a spike. The reason for the overlapping of the ranges is to be able to remove spikes that cross two depth ranges with different settings.

4. The time-varying ambient noise was quantified and corrected according to Korneliussen (2000). The measured samples were corrected by subtracting the estimated average noise for the measured sample, and by removing all samples that were weaker than the estimated high noise cut-off. This means that all measurements that were so weak that they were inside the noise pdf (probability density function) were set to zero, and all stronger measurements were reduced by the estimated average noise.

The pre-processed data were further scrutinized in the water column down to 1000 m using LSSS (Korneliussen et al., 2006, 2016). The density estimates were checked using echo counting, as described by Mitson and Wood (1961), later refined by Kieser and Mulligan (1983), and for target strength (TS) measurements by Ona and Hansen (1986). Most single targets and single-target tracks were detected in the mesopelagic layer at 300–450 m depth and only few below 600 m. Apart from intervals at a few stations, the epipelagic layer (the upper 300 m) was much noisier than the mesopelagic layer. Backscatter measurements within the first 0.4 s after transmission were generally noisier than those made in the period after 0.4 s. There was intermittent noise interference in the top 300 m of the water-column that was likely due to instruments on-board the ship. During periods where the noise was absent, the density of targets above 300 m seemed to be much lower than between 300 and 600 m. Unfortunately, the consistency of the target density above 300 m could not be assessed due to the intermittent noise. The data were stored in the LSSS database as vertical profiles with 10 m depth resolution where each profile was averaged over 25 pings.

The acoustic equipment was calibrated on-board *IB Oden* on 1 September 2015, following a standard methodology described by Foote et al. (1981). This was a centre calibration with a CU64 mm sphere, where the data were collected within 1 degree off axis. Examination of the calibration results showed that data collected at pulse lengths of 8, 4, and 2 ms were acceptable, whereas data for 1 ms pulse length could not be used due to an "overshoot" in amplitudes in the spectrum. The results showed a large calibration offset of >10 dB, with correction factors of 11.5, 12.0, and 15.8 for backscattering obtained with pulse lengths of 8, 4, and 2 ms. The corresponding corrections for individual TS were −5.3, −5.4, and −6.0 dB at the same pulse lengths (Table 1). Since the calibration was performed one year before the measurements were made, we tested the stability of the Simrad EK80, 18 kHz, system onboard *IB Oden* by comparing the 2015 calibration with a later calibration in 2019, in both cases using the same pulse duration and power. The calibration was performed on the data processed as described above, with noise removal and filtering the outer parts of the FM data. The change in Gain (G_0) for echo integration and TS measurements, as defined in the equations of Ona et al. (2009), was only 0.6 dB weaker in 2019 compared to 2015. Also, the impedance of the four quadrants of the BITE menu of the EK80 software system was monitored and found equal in 2015 and 2019. The observed variation in gain from 2015 and 2019 was a bit larger than reported by Knudsen (2009) for 18 kHz systems, but within acceptable range. Based on our evaluation, we conclude that the data collected in 2016 is valid with the accuracy of ± 1 dB for both the Nautical Area Scattering Coefficient (NASC) and TS measurements, corresponding to ± 25% in density and backscattering cross section, derived from mean TS.

2.4. Acoustic data sets

Firstly, a "Full data set" (Data S1) was built by calculating NASC in $m^2\,nmi^{-2}$ (Foote and Knudsen, 1994; MacLennan et al., 2002; Simmonds and MacLennan, 2005). To discriminate backscatter from fish or other organisms with similar target strength from background noise and weak echoes from plankton organisms, the minimum echo integrator threshold in terms of the volume backscattering strength (s_v) was gradually increased from the default setting of −82 dB to about −75 dB when most echoes from distinct single targets (Fig. S2c) remained but background noise and echoes from smaller organisms disappeared from the echograms.

Secondly, a "Target-tracking data set" (Data S2) was built by using a target-tracking algorithm, containing only the NASC that emerged from single-target tracks. The ES18-11 is a split-beam transducer, divided into four quadrants, so all targets in the beam giving an echo can be positioned in the beam. Following the position of a target over consecutive pings and adjusting for vessel movement allows for calculating the movement (speed and direction) of the targets. Single point targets were detected and connected into individual tracks according to the target-tracking method proposed by Handegard et al. (2005). Tracking individual targets allowed us to discern among backscatter from organisms and noise occurring as spikes. To be accepted as valid, a track was required to contain at least eight detections. A track was accepted if <30%, and not more than five consecutive pings, missed detection (Fig. S2b). Visual inspection showed that LSSS was able to track the specimens with these settings. The tracks were transformed into areas tightly surrounding the tracks in LSSS and the backscattering, in the form of NASC, from these areas was integrated and transferred to data files. Since target tracking is not very efficient in the shallower parts of the water column where the beam is narrow, the backscatter from depths less than ca. 300 m, i.e., received at times less than ca. 0.4 s, will mostly be lost. An investigation of a data subset showed that reducing the number of pings allowed missing from a track from 5 to 1 increased the number of tracks, but NASC did not change much (5%).

The "Full data set" included higher total NASC than the "Target-tracking data set" at Stations 1–5 and 9, and a part of Station 6 (Fig. S3b), which could be attributed to noise that passed the pre-processing filtering and were interpreted as real echoes. The total NASC values in the "Target-tracking data set" may be considered more reliable, since the criteria for accepting an echo as part of a track from a real scattering object were very strict (Fig. S2). We therefore consider the "Target-tracking data set" to contain minimum estimates of the backscattering objects. There is some uncertainty as to whether the "Full data set" can be considered maximum estimates since the noise-reduction may also have removed some of the true backscatter along with the noise. We therefore consider the values in the "Full data set" as "high", but not maximum.

2.5. Target strength

In the present study neither species nor lengths are known. Consequently, the *in situ* target strength (TS) distribution estimated from the echosounder output (corrected for position in the beam) was used to calculate areal densities of scatterers. For most fish possessing a swim bladder, the TS varies with frequency. Fishes with swim bladders and similar size and morphology will, however, act as similar targets at 18 and 38 kHz. For another similar-sized gadoid fish *Trisopterus esmarkii*, the frequency response was found to be relatively flat (r(f) = 1) over a frequency range between 16 and 20 kHz to 38 kHz (Pedersen and Korneliussen, 2009). Consequently, we made no recalculation of the NASC from 16–20 to 38 kHz. To avoid TS distributions being biased towards higher values due to reduced signal-to-noise ratio in the outer parts of the beam, only TS measurements close to the acoustic axis (within 2°) were extracted.

2.6. Oceanographic data collection

During the "Arctic Ocean 2016" expedition with *IB Oden*, CTD data

were collected with a SeaBird 911 equipped with dual SeaBird temperature (SBE 3) and conductivity (SBE 04 C) sensors. CTD measurements were available for 12 of the 13 acoustic sampling stations (Table 1). At one station, Station 4 at the Lomonosov Ridge (Fig. 1), no CTD was operated (Gårdfeldt and Lindgren, 2016). The CTD measurements for Station 1 were taken nearby the acoustic sampling station, but some weeks later. For the water in the mesopelagic layer (300–600 m), these latter measurements should be comparable for August and September as the deep water is isolated from the influence of the atmosphere and has rather stable conditions as shown by, e.g., year-long instruments deployed north of Svalbard (Renner et al., 2018). For the surface waters on the other hand, measurements a few weeks off in time in the CAO are not comparable as this layer is subject to both seasonal and short-time variability.

3. Results

3.1. Detection of a DSL

Along part of the transect, from Station 1 to Station 7, a distinct DSL at 300–600 m of water depth was clearly documented, while it was more diffuse – but present – from Station 8 to Station 13 (Figs. 1 and 2a). Using the target-tracking possibilities of the split-beam transducer, we observed that individual targets were moving in the acoustic beam with speeds of up to 13 cm s^{-1}, showing that they were living organisms (Fig. S2b). Schools of organisms did not occur in the data set and single target-tracking was possible for all data.

The mean NASC per station for the 300–600 m layer varied between 0.02 and 1.88 m^2 nmi^{-2} in the "Target-tracking data set" and between 0.02 and 7.04 m^2 nmi^{-2} in the "Full data set" (Table 2, Fig. S3b). The mean NASC was highest at the two stations closest to the North Pole (Stations 2 and 5), intermediate in the Amerasian Basin (Stations 6 and 7), and lowest near the Gakkel Ridge and in the Nansen Basin (Stations 11–13). Furthermore, the NASC was clearly concentrated between 300 and 600 m of depth at the North Pole, the Lomonosov Ridge, and in the Amerasian Basin, while near the Gakkel Ridge and in the Nansen Basin the NASC was more evenly distributed over the whole water column between 50 and 950 m (Fig. S4). In the Amundsen Basin (Stations 1, 9, 10), the DSL was most pronounced at 300–400 m of depth.

While our NASC data can be trusted for the 300–600 m stratum, they could be underestimated for the upper 300 m where the acoustic backscatter was often obscured by noise. However, time windows when this noise was absent or low suggest that the NASC were generally much lower in the upper 0–300 m layer than in the 300–600 m layer, providing distinctness to the DSL (Fig. 2).

3.2. NASC and water temperature

Along the whole transect studied, the central Arctic DSL coincided with the "Atlantic water layer". This deeper layer of warmer, saltier water delivered to the CAO from the Atlantic Ocean is located below the colder upper mixed layer and the halocline (Figs. 3 and S5). The DSL

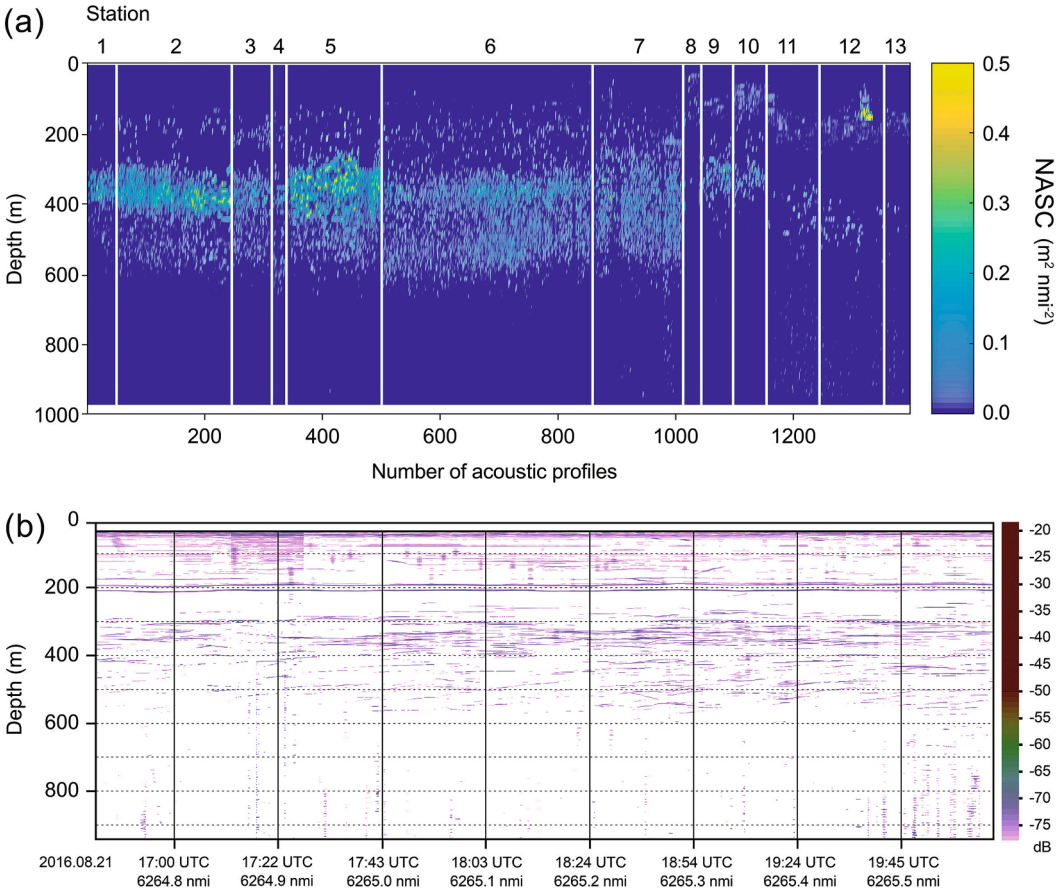

Fig. 2. The deep scattering layer (DSL) between ca. 300 and 600 m of depth in the Central Arctic Ocean (CAO). (a) Vertical distribution of the area scattering coefficient (NASC) in the upper 1000 m of the water column in the 1,363 acoustic profiles at Stations 1–13 (Fig. 1). The white vertical lines in the graph delimit the stations. Note that, due to noise, the data for 0–300 m may be underestimated. (b) Echogram showing the distinctness of the DSL between ca. 300 and 600 m at the North Pole (89.98 °N, 71.69 °E; Station 5) on 21 August 2016 from the Large-Scale Survey System (LSSS; Korneliussen et al., 2016) at 18 kHz and volume backscattering strength threshold (S_v) = −78 dB re 1 m^{-1}. This echogram covers water-column depth 20–940 m along a 0.85 nmi long track during a 3.5-hour time window when disturbances by noise in the upper part of the water column (above 300 m) were relatively low compared to the larger part of the acoustic dataset.

Table 2
The mean area scattering coefficient (NASC) and target strength (TS) measured in the deep scattering layer (300–600 m), and body length, density and biomass calculated from NASC and TS assuming that the acoustic backscatter originates from the small endemic Arctic gadoids *Boreogadus saida* and/or *Arctogadus glacialis*. Values are given for both for the "Target-tracking data set" and the "Full data set". Body length was calculated using the empirical relationship between TS and body length for *Boreogadus saida:* $TS = 21.8\ log_{10}\ L - 72.7$ proposed by Mamylov (1988). Stock density and biomass were calculated using the NASC, TS, and the length-weight relationship for *Boreogadus saida* (Fig. 6). The density calculations were based on the measured TS values for Stations 1–6, but when <100 TS data points were measured in a specific depth layer at a specific station (Stations 7–13) the mean TS of all data (-46.8, n = 13,667; Fig. 5a) was used.

Acoustic sampling station	Location	Mean NASC (m^2 nmi^{-2})		Mean TS (dB)	Mean body length (cm)	Mean density (individuals km^{-2})		Mean biomass (kg km^{-2})	
		Target-tracking data set	Full data set			Target-tracking data set	Full data set	Target-tracking data set	Full data set
1	Amundsen Basin	0.65	1.19	−47.0	15.1	752	1381	16.3	30.0
2	North Pole	1.31	2.37	−47.1	14.9	1568	2836	32.7	59.1
3	Lomonosov Ridge	0.69	3.16	−46.0	16.8	637	2911	19.1	87.2
4	Lomonosov Ridge	0.48	1.07	−45.8	17.1	425	939	13.4	29.7
5	North Pole	1.88	4.04	−46.6	15.7	2021	4331	49.4	105.8
6	Amerasian Basin	0.86	1.24	−50.4	10.5	2160	3119	15.7	22.6
7	Amerasian Basin	0.84	0.82	−46.8	15.4	935	911	21.5	21.0
8	Amerasian Basin	0.09	0.09	−46.8	15.4	99	96	2.3	2.2
9	Amundsen Basin	0.33	7.04	−46.8	15.4	371	7826	8.5	180.3
10	Amundsen Basin	0.19	0.19	−46.8	15.4	214	214	4.9	4.9
11	Gakkel Ridge	0.08	0.08	−46.8	15.4	92	92	2.1	2.1
12	Nansen Basin	0.06	0.06	−46.8	15.4	65	65	1.5	1.5
13	Nansen Basin	0.02	0.02	−46.8	15.4	22	22	0.5	0.5
Mean for n = 13 stations						**720**	**1903**	**14.5**	**42.1**

extended along the transect from ca. 150 m of depth in the Nansen Basin and ca. 220 m in the Amerasian Basin down to ca. 700 m of depth (Figs. 3a and S4). The water temperature at 300–600 m spanned the range 0.3–1.6 °C, being lowest in the Amerasian Basin (0.3–0.9 °C), highest in the Nansen Basin (0.7–1.6 °C), and intermediate in the Amundsen Basin and North Pole area (0.3–1.2 °C) (Figs. 3a and S5a). Salinity was lower above the Atlantic water layer (Figs. 3b and S5b), but showed only marginal differences between the stations at 300–600 m of depth (range 34.8–34.9). Also oxygen concentration (6.4–6.8 mL L^{-1}) and water density (1029–1031 kg m^{-3}) varied only marginally among stations in this depth interval (Fig. S5c,d).

The highest NASC was recorded at or below the depth of the temperature maximum in the North Pole area, the Amerasian Basin, and the Amundsen Basin (Figs. 3a and S5). The Nansen Basin differed from the other areas of the CAO studied by higher temperatures and higher NASC both higher up and deeper down in the water column (Figs. 3a and S4). >99% of the backscattering organisms in the DSL had ambient temperature within the range 0.4–1.2 °C, thus covering most of the temperatures within the 300–600 m depth range (0.3–1.6 °C). When comparing the distributions of ambient temperature and the temperatures available to the organisms in the same water layer, it appeared that the organisms were more concentrated at 1.0–1.2 °C than at 0.4–0.7 °C (Fig. 4). The distribution of ambient temperatures is skewed towards the warmer end with >80% of the organisms residing in waters with temperature 0.7–1.2 °C while this range covers only 55% of the temperature range within the DSL.

3.3. Target strength (TS) from single targets

Numerous tracks of single targets were detected in the DSL, providing good TS estimates that suggest the occurrence of fish-sized organisms (Data S3), and the acoustic records consisted of pronounced traces resembling those of fish (Figs. 2b and S2c). The TS data in the depth span 0–600 m ranged between −69.9 and −38.6 dB (N = 13,667 data points) with a mean value of −46.8 dB (based on σ_{bs}), and were completely dominated by data from 300 to 600 m depth. Very few TS data (only 372 data points) were recorded in the upper 300 m, the uppermost one at 166 m. The frequency distribution of the TS values is unimodal and appears like a slightly skewed normal distribution (Fig. 5a); 50% of the distribution represented values between −48.9 and −45.8 dB, and 90% of the distribution represented values between −51.6 and −44.6 dB. There was a trend of increasing TS values with increasing depth by about 3 dB for the core of the data points (Fig. 5b). This could indicate the occurrence of slightly larger objects at greater depth although this could also be an artefact due to the detection level increasing with increasing distance to the target.

4. Discussion

4.1. The CAO has a DSL with low abundances of organisms

Our study suggests that a DSL is a common and widespread feature in the mesopelagic zone of the CAO, at least in summer, because we detected this layer along our whole transect in August-September. Similar structures have been observed in the Svalbard area just south of the CAO – both in open water and below sea ice – in 2014 (Knutsen et al., 2017), 2015 (Gjøsæter et al., 2017), 2016 and 2017 (Geoffroy et al., 2019), and in September 2017 across the entire Fram Strait from Svalbard to Greenland (Gjøsæter et al., 2020). The hitherto northernmost reported DSL was detected under the ice cover in the Sofia Deep at 82.1 °N (Gjøsæter et al., 2017, Fig. 1).

The abundance of the organisms in the central Arctic DSL is low. The mean NASC (300–600 m) of up to 2 m^2 nmi^{-2} with target tracking and up to 7 m^2 nmi^{-2} without target tracking, is several orders of magnitude lower than those reported from the northern Atlantic Ocean. For example, the mean NASC (0–800 m) in the open ocean part of the Irminger Sea was found to vary between 319 and 1845 m^2 nmi^{-2} (Anderson et al., 2005), and in the Norwegian Sea the mean NASC (0–1000 m) varied between 66 and 365 m^2 nmi^{-2} (Knutsen et al., 2017). The Atlantic DSL was found to decrease north-westward from a mean

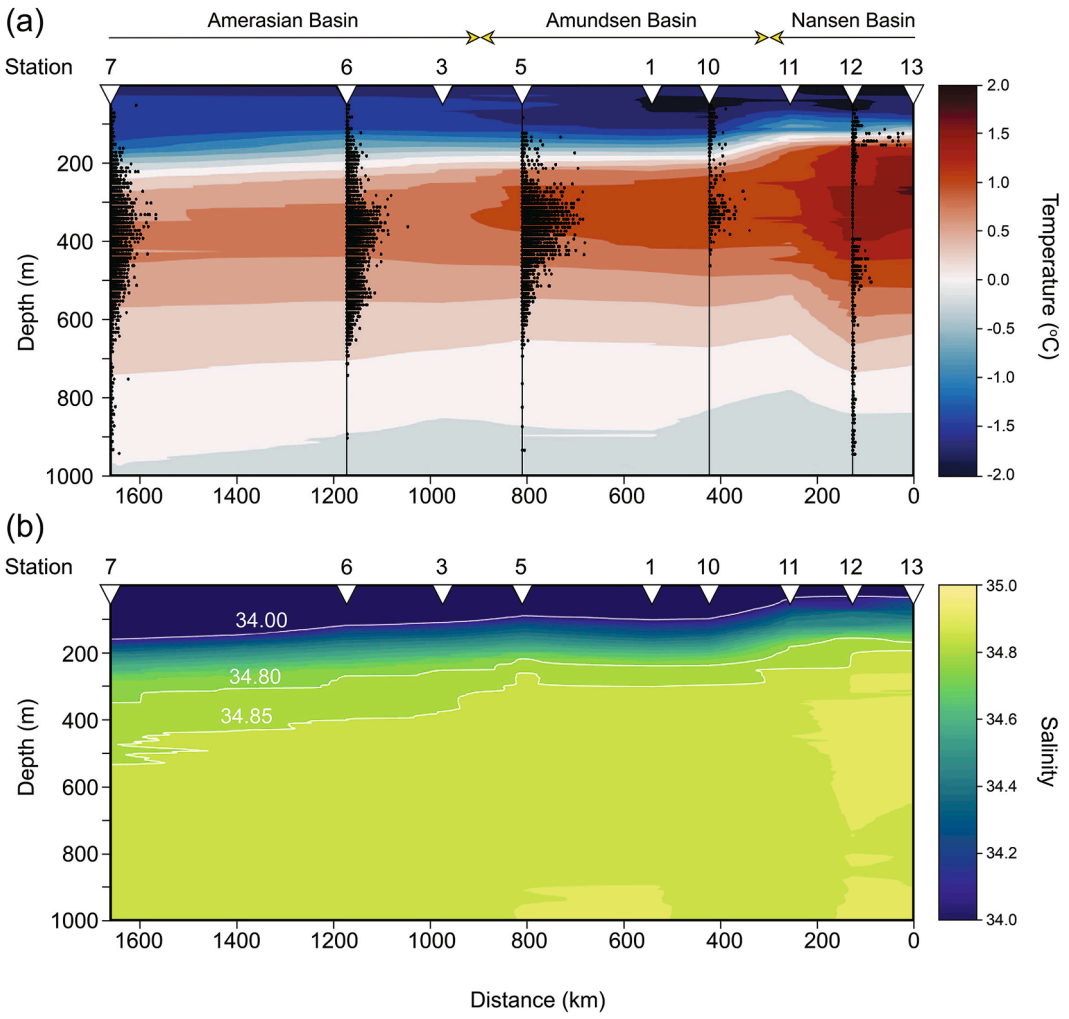

Fig. 3. Vertical distributions of temperature and salinity in the water column based on CTD measurements from nine of the sample stations along the transect in the Central Arctic Ocean (CAO). (a) Vertical distributions of temperature and the area scattering coefficient (NASC) based on the "Target-tracking data set" (Fig. S3). Plots for the NASC at all 13 stations are shown in Fig. S4. (b) Vertical distribution of salinity. Not used in the construction of these plots are: Station 2 (North Pole, values almost identical to Station 5), Station 4 (no CTD data available), and Stations 8 and 9 (marginal to the transect) (Fig. 1). The resolution in some parts of the transect, in particular in the Amerasian Basin, is low due to the low number of stations. The plot was made in Matlab R2016.

NASC (0–900 m) of ca. 360 m^2 nmi^{-2} in the eastern Norwegian Sea down to ca. 15 m^2 nmi^{-2} in the colder waters north of Iceland (Norheim et al., 2016). Similarly, the mean NASC in the DSL (200–800 m) decreased northward from 215 m^2 nmi^{-2} in the Norwegian Sea to 61 m^2 nmi^{-2} west of Svalbard (Siegelman-Charbit and Planque, 2016). However, the low NASC recorded in the DSL north of Svalbard in the Sofia Deep (ca. 5 m^2 nmi^{-2}) and at the Yermak Plateau (ca. 7 m^2 nmi^{-2}) are comparable to the highest values recorded in our study in the CAO (Gjøsæter et al., 2017). In the former study, the DSL was found at ca. 150–720 m with temperature 1.2–1.5 °C, and this – together with the present study – suggests that the DSL this far north coincides with the Atlantic water that enters the Arctic Ocean via Fram Strait and the Barents Sea (Rudels, 2019). The higher NASC in the warmest part of the vertical water column may be due to temperature preference in combination with light penetration (Schauer et al., 2002; Aksnes et al. 2017).

4.2. Possible identity of the organisms in the DSL

Our data provide a first indication of possible mesopelagic fish under the pack-ice cover of the Arctic Ocean. However, our data have two drawbacks with respect to the identity of the targets in the central Arctic DSL-: (1) no samples of organisms were taken, which implies that the acoustic backscatter could not be verified with information on the taxonomic composition of the pelagic fauna, and (2) since the acoustic backscatter was measured over a single narrow frequency band, we could not separate the backscatter from organisms with gas inclusions from organisms without. DSLs at mesopelagic depths usually consist of a mixture of small mesopelagic fishes, crustaceans, cephalopods and gelatinous zooplankton (Irigoien et al., 2014; Klevjer et al., 2016). In agreement with this, the DSL immediate south of the CAO is known to contain the small fishes polar cod (*Boreogadus saida*), juvenile beaked redfish (*Sebastes mentella*), spotted barracudina (*Arctozenus risso*), the lanternfishes (myctophids) *Benthosema glaciale* and *Lampanyctus macdonaldi*, the squid *Gonatus fabricii*, and large zooplankton such as krill, amphipods and gelatinous species (Gjøsæter et al., 2017; Geoffroy et al., 2019). Small fishes have to our knowledge never been caught in zooplankton nets in the CAO, possibly because they tend to avoid nets (Sameoto et al., 2000).

If we assume that the organisms moving in the acoustic beam with speeds of up to 13 cm s^{-1} and with TS values between −69.9 and −38.6 dB are small fishes with gas bladders, plausible candidates are the two endemic Arctic gadoids, polar cod *Boreogadus saida* (Mueter et al., 2016) and ice cod *Arctogadus glacialis* (Jordan et al., 2003), both single species in their genus and hereafter referred to as "*Boreogadus*" and "*Arctogadus*". These two species are known to have circumpolar distributions and

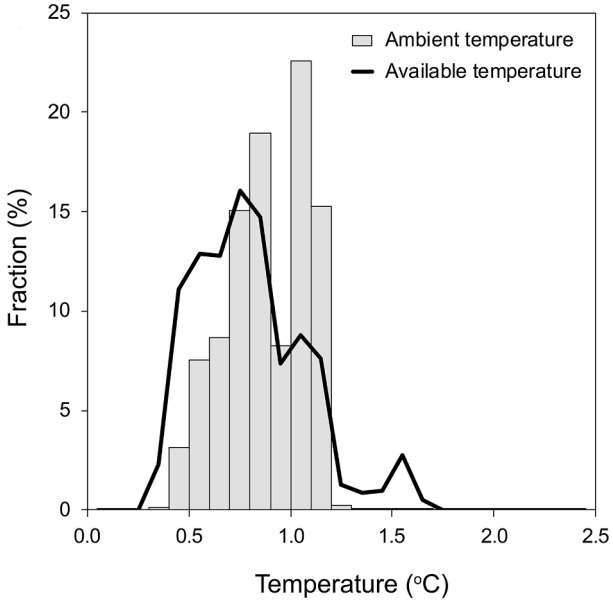

Fig. 4. Distributions of ambient temperature for the organisms and temperatures available to the organisms in the 300–600 m depth layer from 12 stations out of 13 (no temperature data were available for Station 4; Table S1). The ambient temperature for the organisms in the 300–600 m depth layer was calculated for each station by weighting the observed temperatures with area scattering coefficients (NASC) from the "Target-tracking data set". The calculations were conducted for 10-m depth intervals (corresponding to the resolution of the NASC) and binned into 0.1 °C temperature intervals. The temperatures available to the organisms was calculated using the same method but without weighting. The two distributions would be the same if the organisms would be distributed evenly in the 300–600 m depth layer.

known to occur associated with the pack ice in the CAO (Andriashev et al., 1980; Gradinger and Bluhm, 2004; Melnikov and Chernova, 2013; David et al., 2016; Bluhm et al., 2017). Other circumpolar nekton that has been recorded in the CAO is the up to ca. 30 cm long squid *Gonatus fabricii* (Nesis, 1971, 2001; Young, 1973). In the Norwegian Sea, larger individuals (>20 cm) of this species are seemingly restricted to depths between 400 and 1200 m (Arkhipkin and Bjørke, 1999 and references therein). However, due to lack of gas inclusions, and only a soft chitinous pen embedded in its body tissue, this squid would give much weaker echoes at 18 kHz than a similar-sized *Boreogadus* or *Arctogadus*.

The assumption that the DSL would include small gadoids could be considered reasonable because *Boreogadus* occurs in high abundances – and is a key species – in the marine pelagic food webs of the Arctic shelf seas surrounding the CAO (Geoffroy et al., 2011; Hop and Gjøsæter, 2013; Logerwell et al., 2015; Mueter et al., 2016; De Robertis et al., 2017) and *Boreogadus* juveniles are ubiquitous in the sea-ice habitat throughout the CAO (David et al., 2016 and references therein). *Arctogadus* has a circumpolar shelf distribution as well, but is apparently less abundant than *Boreogadus* (Aschan et al., 2009; Mecklenburg et al., 2018). Unique observations of both species were made from Soviet winter stations drifting with the sea ice in the Amerasian Basin near the Mendeleyev Ridge in the 1950s–1970s (Andriashev et al., 1980), where hundreds of individuals of these two gadoids were caught with hooks down to 25 m. In November-December most of the fishes were 10–20 cm long, but in February-March larger individuals (up to 43 cm) identified as *Arctogadus* were also caught. The specimens of *Boreogadus* that were caught rarely exceeded 15–17 cm.

The overall depth distribution of *Arctogadus* in the European Arctic ranges from 155 to 741 m, with most observations at depths of 300–400 m (Aschan et al., 2009). This would agree with the vertical distribution of the DSL in the CAO we discovered. A tentative suggestion that needs validation in future studies is that *Arctogadus* is a true pelagic species living at mesopelagic depth in the Atlantic layer of the CAO. The early studies from Soviet ice-drift stations showed that *Arctogadus* can occur associated with the sea ice in the CAO in winter (Andriashev et al., 1980), where they can feed on ice amphipods and juvenile *Boreogadus*. When the light returns in spring, *Arctogadus* would then descend to deeper water.

For *Boreogadus* a "sea-ice drift" hypothesis has been suggested for its transport from coastal spawning areas to the Amerasian and Eurasian Basins (Melnikov and Chernova, 2013; David et al., 2016). Young-of-the-year from spawning areas in the Russian shelf seas would, according to this hypothesis, become associated with sea ice when it forms in autumn and then passively be transported to the CAO with the transpolar ice drift (Spall, 2019). Juvenile *Boreogadus* feed on ice-associated invertebrates, mainly amphipods, and can hide from predators in crevices in the ice (David et al., 2016). Based on our discovery of the central Arctic DSL, we could extend the hypothesis to include the possible descent of *Boreogadus* to the mesopelagic zone of the CAO when they grow older and forage on the crustaceans that dominate the zooplankton

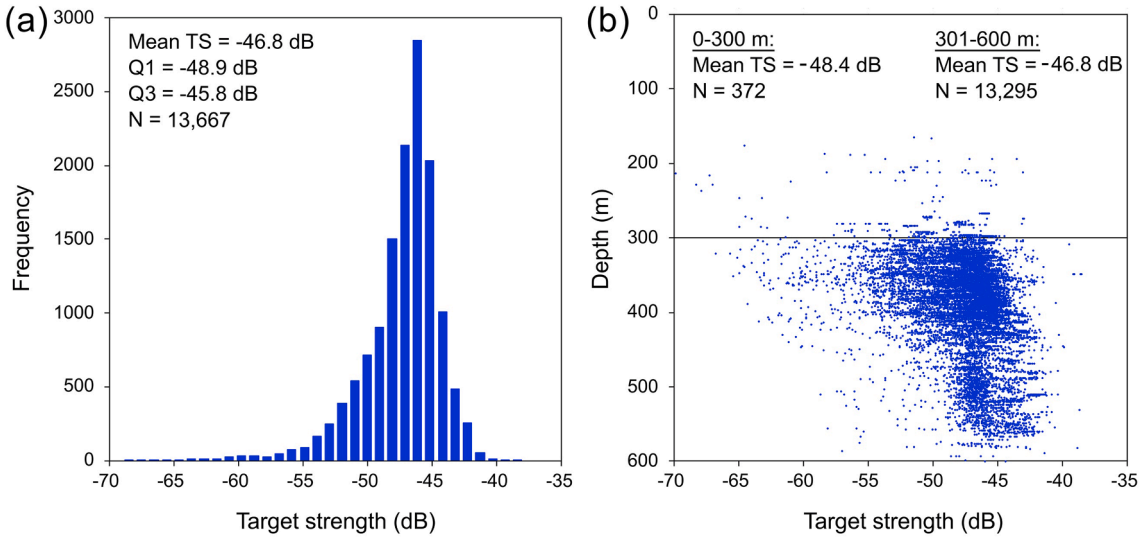

Fig. 5. The target strength (TS) at 0–600 m of depth at Stations 1–13 (Fig. 1). Only TS data from within 2° of the beam axis are included. (a) Histogram with mean and quartiles 1 and 3 (Q1 and Q3) for all 13,667 TS data points. (b) The relationship between all TS values and water depth, including separate mean TS values for 0–300 m and for 300–600 m, respectively.

communities in the mesopelagic zone of the CAO (Kosobokova et al., 2011), as a coupling between shallow and mesopelagic ocean habitats. Data from the Beaufort Sea show *Boreogadus* to be vertically segregated by size in all months, with juveniles in the epipelagic (<100 m deep) layer and older *Boreogadus* in the Atlantic layer along the slopes of the Beaufort Sea at 200–500 m depth (Benoit et al., 2014; Geoffroy et al., 2016). It has been suggested that early hatching (already in January) enables the juvenile fish to reach a minimum size and capacity to avoid predation before they join their cannibalistic congeners in the mesopelagic Atlantic layer as larger individuals (Bouchard and Fortier, 2011). This strategy could be the same in the CAO with juveniles associated with sea ice (Gradinger and Bluhm, 2004; Melnikov and Chernova, 2013; David et al., 2016) and adults deeper down.

However, we must consider that (part of) the acoustic backscatter in our data could originate from pneumatophores (gas-filled floats) of physonect siphonophores (colonial hydrozoans). The pneumatophore is situated at the top of the colony to provide buoyancy and may be detected acoustically depending on frequency, depth, and size of the gas inclusion. Furthermore, physonect siphonophores are equipped with nectophores (swimming bells) that allow excellent motility (Costello et al., 2015). Many physonect siphonophores are known to inhabit the mesopelagic domain globally, and it has been argued that their contribution to backscatter must be determined to obtain better estimates of mesopelagic fish in the world's oceans (Proud et al., 2018). The physonect siphonopore *Marrus orthocanna*, an orange-coloured Arctic species with colony length of up to 2–3 m (R. R. Hopcroft, pers. comm.), is present in the CAO and the deep Beaufort Sea (Raskoff et al., 2010; Kosobokova et al., 2011). Another Arctic physonect siphonophore, *Rudjakovia plicata*, has been recorded in the CAO (Margulis, 1982; Kosobokova et al., 2011). *R. plicata* is not very well known (Mapstone, 2014), but is probably more abundant than initially thought (R.R. Hopcroft, pers. comm.; Raskoff et al. 2010; Kosobokova et al., 2011). Other zooplankton organisms, like chaetognaths, amphipods, pteropods, ctenophores and calycophoran siphonophores (without pneumatophore), are very weak scatterers with the exception of the pteropods, but these are mainly epipelagic (Kobayashi, 1974) and are seldom found at DSL depths. The echo returns at 18 kHz of the copepod *Calanus hyperboreus* and other similar-sized crustaceans that dominate the mesozooplankton biomass in the CAO (Kosobokova et al., 2011), are several orders of magnitude below what was observed in this study, and will most certainly not be detected at this frequency.

4.3. Maximum possible mesopelagic fish biomass

Catch data, including species identification and body size, are necessary for estimating fish density and biomass from NASC data. Since traditional trawling for fish sampling under the pack ice is impossible, it will probably take a long time before such data can be collected in the North-Pole area. By assuming that the individual tracks in the central Arctic DSL represent the endemic Arctic gadoids *Boreogadus* and/or *Arctogadus*, a rough estimate of maximum possible mesopelagic fish stock can be calculated from our NASC data. However, the true density and biomass of fish is lower and cannot be quantified from this dataset due to backscatter originating from pneumatophores of physonect siphonophores (Raskoff et al., 2010; Kosobokova et al., 2011).

Our unimodal TS frequency distribution within a narrow TS range indicates a relatively homogenous composition of the 13,667 individual targets. By applying the TS-length relationship for *Boreogadus* proposed by Mamylov (1988), this results in a hypothetical average body length of 15.4 cm. In the North-Pole area (Stations 1–5), the average body length would be ca. 15–17 cm, and in the Canada Basin (Station 6) ca. 10.5 cm (Table 2). These lengths agree with literature data on the known lengths of *Boreogadus* and *Arctogadus* in the Arctic shelf seas surrounding the CAO (Fig. 6). The length-age models are very similar for *Boreogadus* and *Arctogadus* up to the age of about 2 years, but after that *Arctogadus* grows faster and can become twice as old and twice as long as *Boreogadus* (Christiansen et al., 2012; Nahrgang et al., 2014). If the acoustic backscatter in our data set would originate from *Boreogadus*, 80% of the fishes would be 1.8–4.7 years old and weigh 5–47 g, and if it would originate from *Arctogadus*, 80% of the fishes would be 1.5–3.6 years old and weigh 5–54 g (Table 3). Thus, the central Arctic DSL would largely be inhabited by a mixture of late juveniles and adults. However, it should be kept in mind that *Boreogadus* and *Arctogadus* are not the only fish candidates, e.g., the occurrence of myctophids (Gjøsæter et al., 2017) cannot be excluded.

Continuing with the assumption that the individual tracks in the DSL of the CAO represent *Boreogadus*, *Arctogadus*, or both, the maximum possible ranges of fish density and biomass in the central Arctic DSL would be 22–2200 individuals km^{-2} and 0.5–50 kg km^{-2} (Table 2). This is on average 720 individuals km^{-2} and 14.5 kg km^{-2} based on the "Target-tracking data set" or 1900 individuals km^{-2} and 42 kg km^{-2} based on the "Full data set" (n = 13 sampling stations). From these numbers it can be concluded that – if we have a mesopelagic stock of fish with swim bladders in the CAO – it is widespread but very small. For comparison, the total stock biomass of *Boreogadus* in the 1.4 million km^2 Barents Sea was on average 777,000 tons in the period 1986–2017 (555 kg km^{-2}) with a maximum of 1.94 million tons in 2006 (1,386 kg km^{-2}) (van der Meeren and Prozorkevich, 2019). We emphasize that there is considerable uncertainty in our estimate for the CAO due to limited spatial coverage of our data with only one transect, only one summer month (15 August-15 September), the potential masking of backscatter by noise, and the possible contribution of siphonophores to the acoustic backscatter. Our density and biomass estimates are in the same order of magnitude as previous estimates of juvenile ice-associated *Boreogadus* in the sea-ice habitat of 5,000 individuals km^{-2} and 19.3 kg km^{-2} in the Eurasian Basin of the CAO (David et al., 2016), although these calculations were also based on a very limited number of observations in summer.

Our estimated maximum potential biomass of fish in the central Arctic DSL is in broad agreement with the low level of primary production in the CAO. Primary production in the ice-covered waters of the CAO is low, roughly on the order of 10 g C m^{-2} $year^{-1}$ (Gosselin et al., 1997; Olli et al., 2007), which is equivalent to about 100 g wet weight biomass m^{-2} $year^{-1}$. With 10% transfer efficiency between successive trophic levels, this would give an annual production of 1 g m^{-2} $year^{-1}$ (=1000 kg km^{-2} $year^{-1}$) at the tertiary trophic level of planktivorous fish such as *Boreogadus*. This is an order of magnitude higher than our estimate of biomass of fish in the DSL. However, there are several explanations for this discrepancy that probably act in concert: a sizable fraction of the primary production in the CAO goes through the microbial loop, the Atlantic inflow to the CAO transports food items from the Atlantic Ocean to the CAO, and *Arctogadus* is partly at a higher trophic level than the tertiary, being a piscivore consuming juvenile *Boreogadus* (Andriashev et al., 1980). The reason why biomass was highest in the North-Pole area cannot be attributed to primary production; perhaps this is related to the flow of Atlantic water following the Lomonosov Ridge (Rudels 2015).

Indirect support for the occurrence (but low abundance) of a fish stock under the pack-ice is the occurrence (but low abundance) of fish predators in the CAO. The ringed seal *Pusa hispida* is regularly observed from icebreakers, even in the North-Pole area, as well as their predator the hypercarnivorous polar bear *Ursus maritimus* (Reeves, 1998; van Meurs and Splettstoesser, 2003). The diving behaviour of ringed seals is consistent with the depth of the central Arctic DSL, and avoidance of visual predation by mammals may be a possible reason for the DSL to remain at depths of 300–600 m. It has been shown that ringed seals in the Canada Basin can make > 20 dives down to 250–300 m within a few hours (Von Duyke et al., 2019) and they dive on average deeper in the Canada Basin than in the Bering and Chukchi Seas (Crawford et al., 2019). Narwhals *Monodon monoceros* and beluga whales *Delphinapterus leucas* are known to feed on *Boreogadus* and *Arctogadus* (Bluhm and Gradinger, 2008). High numbers (about 1,000 individuals) of narwhals

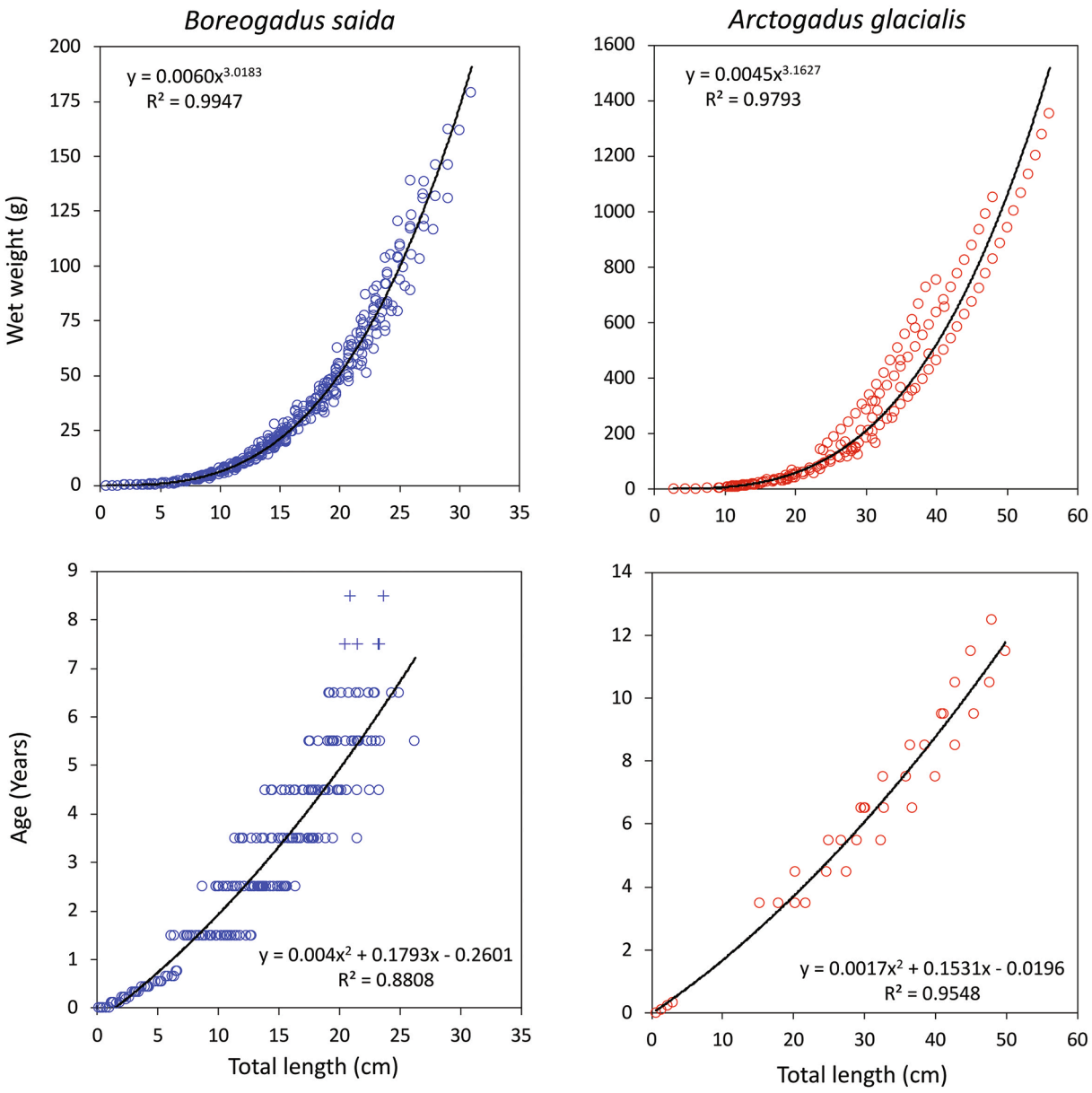

Fig. 6. Length-weight and length-age models for *Boreogadus saida* and *Arctogadus glacialis* based on the publications listed in Tables S2 and S3. The data consist of mean length per age group for adult fish as given in tables and figures in the publications, but for juveniles (<1 year) the age was calculated from published polynomial regressions for each cm fish length in the length interval for which the equation was valid. Since the data were presented in different ways in the publications, the circles represent either primary data, population means or calculated values from published regressions for each cm fish length in the length interval for which the equation was valid. Thus, the R^2 values must be interpreted with care because they are not based on independent measurements. Within publications, data from the same area were treated as one population, and data from different publications were considered as different populations. For *Boreogadus*, fork length (FL) was converted to total length (TL) with the function TL = (1.03724*FL) − 0.0113, valid for the interval 4–30 cm, based on Nahrgang et al. (2014). Standard length (SL) was converted to TL with the function TL = (1.08849*SL) + 0.2736, valid for the interval 5–12 cm, based on David et al. (2016) and further validated up to 17 cm based on SL and TL length measurements in Melnikov and Chernova (2013). For *Arctogadus*, standard length (SL) was converted to total length (TL) with the function TL = (1.1033*SL) − 2.225, valid for the interval 17–41 cm, based on Andriashev et al. (1980) and Borkin and Mel'yantsev (1984).

have been recorded deep into the pack ice in an aerial survey in the western Nansen Basin (Vacquié-Garcia et al., 2017), and in the eastern Nansen Basin this species has been observed north of 85 °N (Belikov and Boltunov, 2002). Beluga whales have been recorded by satellite-tracking to move north to beyond 80 °N in the Canada Basin (Hauser et al., 2014; 2015).

4.4. The possible involvement of siphonophore pneumatophores

It cannot be ruled out that (at least part of) the NASC in our study originated from pneumatophores of physonect siphonophores. The TS of gas bubbles varies with bubble size and depth. Theoretical models show that the TS at 18 kHz for 1.8–3.1 mm diameter gas bubbles, residing at depths between 250 and 700 m, are mainly in the range −60 to −42 dB (Movie S1, Fig. S6), with peak values (resonance) in the range −50 to −40 dB. This is similar to the TS values we recorded in the DSL of the CAO, and siphonophores are therefore a group of organisms that may have contributed to the backscatter in our NASC values. Our conclusion is that with the current theoretical models we cannot separate the backscatter from a 2–4 mm pneumatophore with that from a 2–4 mm gas-filled swim bladder of a fish at 18 kHz.

Unfortunately, there is considerable uncertainty about the size of the

Table 3
Calculations of fish size and age if we assume that the organisms we recorded at TS between −69.9 and −38.6 dB, based on 13,667 TS measurements (Fig. 5a), would be polar cod *Boreogadus saida* and/or ice cod *Arctogadus glacialis*. Body length was calculated using the empirical relationship between TS and body length for *Boreogadus saida: TS = 21.8 log$_{10}$ L – 72.7* proposed by Mamylov (1988). For age and weight, the length-weight relationships for *Boreogadus saida* and *Arctogadus glacialis* in Fig. 6 were used.

Statistic	Target strength (dB)	Total body length (cm)	Age (years)		Weight (g)	
			Boreogadus saida	*Arctogadus glacialis*	*Boreogadus saida*	*Arctogadus glacialis*
Decile 1	−51.6	9.3	1.8	1.5	5.0	5.2
Quartile 1	−48.9	12.4	2.6	2.1	11.8	12.8
Mean	−46.8	15.4	3.5	2.7	23.1	25.7
Quartile 3	−45.8	17.1	4.0	3.1	31.8	36.0
Decile 9	−44.6	19.5	4.7	3.6	46.6	53.7

gas inclusions in physonect siphonophores, and information on how the shape and size of their gas inclusions would vary with depth is lacking as well. For *Nanomia bijuga* with colony size up to 75 cm, average pneumatophore size of 3.27 × 1.16 mm (ca. 1.64 mm ESD = equivalent spherical diameter) and average gas inclusion size of 1.49 × 0.97 mm (ca. 1.12 mm ESD; n = 50) were measured after three weeks fixation in 10% formalin (Barham, 1963). During a siphonophore bloom in a fjord system in northern Norway it was found that high abundance of *Nanomia cara* was reflected in the acoustic backscatter at 18, 38 and 120 kHz in the water column slightly deeper than 300 m (Knutsen et al., 2018). Associated with the latter observations, a small number of pneumatophore diameters were measured, and the largest pneumatophore had an ESD of 1.12 mm, measured in formalin-conserved material about three weeks after collection (T. Knutsen, pers. comm.).

Of the two physonect siphonophore species that have been recorded in the CAO (Raskoff et al., 2010; Kosobokova et al., 2011), the colonies of *Marrus orthocanna* are larger (up to 2–3 m) than those of the two *Nanomia* species mentioned above, while the colony of *Rudjakovia plicata* (Margulis, 1982) is only up to 10–15 cm long (R.R. Hopcroft pers. comm.). The largest *Marrus orthocanna* colonies may have an estimated pneumatophore size of up to 5–10 mm in diameter (R.R. Hopcroft, pers. comm.). However, this and other species' pneumatophore sizes needs verification from *in situ* measurements. For the related species *Marrus claudanielis* two preserved pneumatophores measured 5.0–5.2 × 1.6–1.7 mm (ca. 2.46 mm ESD; Dunn et al., 2005). Altogether, it is evident that physonect siphonophores inhabit waters that overlap with the DSL we discovered in the CAO, and that presently it cannot be excluded that these siphonophores could contribute with acoustic backscatter of similar TS as small mesopelagic fish.

5. Conclusions

Despite great reduction of the sea-ice cover in the CAO, the area is still inaccessible for fishing vessels, preventing both commercial harvesting of fish and standard data collection for assessment of its fish stocks. Although we were not able to establish with certainty that the central Arctic DSL contains mesopelagic fishes, we discovered a clear DSL that is a typical habitat for zooplankton and small fishes worldwide. In the low-productive CAO ecosystem, the hypothetical fish in the DSL are likely to have a key role in the food web, providing a high-energy lipid-rich resource to higher trophic levels, such as narwhals, seals and polar bears, allowing mammals to survive even in the North-Pole area. An essential research priority is to sample organisms from the central Arctic DSL to establish their identity. This will not be an easy task since we found that the organisms are extremely sparse, relatively small, and possibly too fast to be caught in nets. From our study we can conclude that if the central Arctic DSL contains fish, their biomass is currently too low for any sustainable fishery. Northern fisheries are much more profitable south of the CAO in the Arctic shelf seas and sub-Arctic seas that are far more productive.

Author contributions

P.S.L. and H.G. conceived the idea. P.S.L. compiled the manuscript; all co-authors contributed to and reviewed the manuscript. Acoustic and CTD data collection was carried out by C.S., L.M., M.J., and K.G. The acoustic data sets were prepared by H.G., R.K., E.O., and T.K. The physiographic classification was made by M.J. Data analyses were carried out by R.I. and P.S.L.

Declaration of Competing Interest

The authors declare that they have no known competing financial interests or personal relationships that could have appeared to influence the work reported in this paper.

Acknowledgements

We thank the Swedish Polar Research Secretariat (www.polar.se) and the crew of *IB Oden* for organizing the logistics during the "Arctic Ocean 2016" cruise, and Russel R. Hopcroft and Maciej K. Mańko for supporting information and discussions on Arctic siphonophores. We acknowledge funding by the Swedish Research Council VR (Research Infrastructures SWEDARCTIC), the Swedish Polar Research Secretariat, and the Research Council of Norway through the project "The Arctic Ocean Ecosystem" (SI_ARCTIC, RCN 228896).

Appendix A. Supplementary material

Supplementary data to this article can be found online at https://doi.org/10.1016/j.pocean.2021.102560.

References

Aksnes, D.L., Røstad, A., Kaartvedt, S., Martinez, U., Duarte, C.M., Irigoien, X., 2017. Light penetration structures the deep acoustic scattering layers in the global ocean. Sci. Adv. 3, e1602468. https://doi.org/10.1126/sciadv.1602468.

Anderson, C.I.H., Brierly, A.S., Armstrong, F., 2005. Spatio-temporal variability in the distribution of epi- and meso-pelagic acoustic backscatter in the Irminger Sea, North Atlantic, with implications for predation on *Calanus finmarchicus*. Mar. Biol. 146, 1177–1188. https://doi.org/10.1007/s00227-004-1510-8.

Andriashev, A.P., Mukhomediyarov, B.F., Pavshtiks, E.A., 1980. On mass congregations of the cryopelagic cod fishes (Boreogadus saida and Arctogadus glacialis) in circumpolar Arctic basins. In: Vinogradov, M.E., Melnikov, I.A. (Eds.), Biology of the Central Arctic Basin. Shirshov Instit. Oceanology, Academy of Sciences, U.S.S.R., pp. 196–211 [in Russian].

Anonymous, 2019. should be EU 2019. Agreement to prevent unregulated high seas fisheries in the Central Arctic Ocean. Official Journal of the European Union L 73, 15.3.2019, pp. 3–8. https://eur-lex.europa.eu/legal-content/EN/LSU/?uri=CELEX:22019A0315(01)).

Arkhipkin, A.I., Bjørke, H., 1999. Ontogenetic changes in morphometric and reproductive indices of the squid *Gonatus fabricii* (Oegopsida, Gonatidae) in the Norwegian Sea. Polar Biol. 22, 357–365. https://doi.org/10.1007/s003000050429.

Aschan, M., Karamushko, O.V., Byrkjedal, I., Wienerroither, R., Borkin, I.V., Christiansen, J.S., 2009. Records of the gadoid fish *Arctogadus glacialis* (Peters, 1874) in the European Arctic. Polar Biol. 32, 963–970. https://doi.org/10.1007/s00300-009-0595-4.

Barham, E.G., 1963. Siphonophores and the deep scattering layer. Science 140, 826–828. https://doi.org/10.1126/science.140.3568.826.

Barnhart, K.R., Miller, C.R., Overeem, I., Kat, J.E., 2015. Mapping the future expansion of Arctic open water. Nat. Clim. Change 6, 280–285. https://www.nature.com/articles/nclimate2848.

Belikov, S.E., Boltunov, A.N., 2002. Distribution and migrations of cetaceans in the Russian Arctic according to observations from aerial ice reconnaissance. NAMMCO Sci. Publ. 4, 69–86. https://doi.org/10.7557/3.2838.

Benoit, D., Simard, Y., Fortier, L., 2014. Pre-winter distribution and habitat characteristics of polar cod (*Boreogadus saida*) in southeastern Beaufort Sea. Polar Biol. 37, 149–163. https://doi.org/10.1007/s00300-013-1419-0.

Bluhm, B.A., Hop, H., Melnikov, I.A., Poulin, M., Vihtakari, M., Collins, E. Gradinger, R., Juul-Pedersen, T., von Quillfeldt, C., 2017. Sea-ice biota. In: CAFF. State of the Arctic Marine Biodiversity Report. Conservation of Arctic Flora and Fauna International Secretariat, Akureyri, Iceland. pp. 33–62. https://www.caff.is/marine/marine-monitoring-publications/state-of-the-arctic-marine-biodiversity-report.

Bluhm, B.A., Gradinger, R., 2008. Regional variability in food available for Arctic marine mammals. Ecol. Appl. 18, S77–S96. https://doi.org/10.1890/06-0562.1.

Bluhm, B.A., Kosobokova, K.N., Carmack, E.C., 2015. A tale of two basins: An integrated physical and biological perspective of the deep Arctic Ocean. Prog. Oceanogr. 139, 89–121. https://doi.org/10.1016/j.pocean.2015.07.011.

Borkin, I.V., Mel'yantsev, R.V., 1984. New data on the distribution of polar cod, *Arctogadus glacialis* (Gadidae), in the Arctic region. J. Ichthyol. 24, 101–103.

Bouchard, C., Fortier, L., 2011. Circum-arctic comparison of the hatching season of polar cod *Boreogadus saida*: A test of the freshwater winter refuge hypothesis. Progr. Oceanogr. 90, 105–116. https://doi.org/10.1016/j.pocean.2011.02.008.

Christiansen, J.S., Hop, H., Nilssen, E.M., Joensen, J., 2012. Trophic ecology of sympatric Arctic gadoids, *Arctogadus glacialis* (Peters, 1872) and *Boreogadus saida* (Lepechin, 1774), in NE Greenland. Polar Biol. 35, 1247–1257. https://doi.org/10.1007/s00300-012-1170-y.

Christiansen, J.S., Mecklenburg, C.W., Karamushko, O.V., 2014. Arctic marine fishes and their fisheries in light of global change. Glob. Change Biol. 20, 352–359. https://doi.org/10.1111/gcb.12395.

Costello, J.H., Colin, S.P., Gemell, B.J., Dabiri, J.O., Sutherland, K.R., 2015. Multi-jet propulsion organized by clonal development in a colonial siphonophore. Nat. Commun. 6, 8158. https://doi.org/10.1038/ncomms9158.

Crawford, J.A., Frost, K.J., Quakenbush, L.T., Whiting, A., 2019. Seasonal and diel differences in dive and haul-out behavior of adult and subadult ringed seals (*Pusa hispida*) in the Bering and Chukchi seas. Polar. Biol. 42, 65–80. https://doi.org/10.1007/s00300-018-2399-x.

David, C., Lange, B., Krumpen, T., Schaafsma, F., van Franeker, J.A., Flores, H., 2016. Under-ice distribution of polar cod *Boreogadus saida* in the central Arctic Ocean and their association with sea-ice habitat properties. Polar Biol. 39, 981–994. https://doi.org/10.1007/s00300-015-1774-0.

De Robertis, A., Taylor, K., Wilson, C.D., Farley, E.V., 2017. Abundance and distribution of Arctic cod (*Boreogadus saida*) and other pelagic fishes over the U.S. Continental Shelf of the Northern Bering and Chukchi Seas. Deep-Sea Res. II 135, 51–65. https://doi.org/10.1016/j.dsr2.2016.03.002.

Ding, Q., Schweiger, A., L'Heureux, M., Battisti, D.S., Po-Chedley, S., Johnson, N.C., Blanchard-Wrigglesworth, E., Harnos, K., Zhang, Q., Eastman, R., Steig, E.J., 2017. Influence of high-latitude atmospheric circulation changes on summertime Arctic sea ice. Nat. Clim. Change 7, 289–295. https://www.nature.com/articles/nclimate3241.

Duarte, C.M., Lenton, T.M., Wadhams, P., Wassmann, P., 2012. Abrupt climate change in the Arctic. Nat. Clim. Change 2, 60–62. https://www.nature.com/articles/nclimate1386.

Dunn, C.W., Pugh, P.R., Haddock, S.H.D., 2005. *Marrus claudanielis*, A new species of deep-sea physonect siphonophore (Siphonophora, Physonectae). Bull. Mar. Sci. 76, 699–714. https://www.ingentaconnect.com/contentone/umrsmas/bullmar/2005/00000076/00000003/art00008#.

FiSCAO, 2017. Final Report of the Fourth Meeting of Scientific Experts on Fish Stocks in the Central Arctic Ocean. Tromsø, Norway, September 26-28, 2016, 82 pp. https://www.afsc.noaa.gov/Arctic_fish_stocks_fourth_meeting/default.htm.

FiSCAO, 2018. Final Report of the Fifth Meeting of Scientific Experts on Fish Stocks in the Central Arctic Ocean. Ottawa, Canada, October 24-26, 2017, 45 pp. https://www.afsc.noaa.gov/Arctic_fish_stocks_fifth_meeting/pdfs/Final_report_of_the_5th_FiSCAO_meeting.pdf.

Foote, K.G., Knudsen, H.P., 1994. Physical measurement with modern echo integrators. J. Acoust. Soc. Japan 15, 393–395. https://www.jstage.jst.go.jp/article/ast1980/15/6/15_6_393/_pdf.

Foote, K.G., Knudsen, H.P., Vestnes, G., Brede, R., Nielsen, R.L. 1981. Improved calibration of hydroacoustic equipment with copper spheres. ICES CM Documents 1981/B:20, 18 pp. http://www.ices.dk/sites/pub/CM Doccuments/1981/B/1981_B20.pdf.

Gårdfeldt, K., Lindgren, Å.,(Eds.), 2016. SWEDARCTIC Arctic Ocean 2016 – Expedition Report. Swedish Polar Research Secretariat, Stockholm. 117 pp. http://polar.diva-portal.org/smash/get/diva2:1081650/FULLTEXT01.pdf.

Geoffroy, M., Daase, M., Cusa, M., Darnis, G., Graev, M., Hernández, Santana, Berge, N. J., Renaud, P.E., Cottier, F., Falk-Petersen, S., 2019. Mesopelagic sound scattering layers of the High Arctic: Seasonal variations in biomass, species assemblage, and trophic relationships. Front. Mar. Sci. 6, 364. https://doi.org/10.3389/fmars.2019.00364.

Geoffroy, M., Majewski, A., LeBlanc, M., Gauthier, S., Walkusz, W., Reist, J.D., Fortier, L., 2016. Vertical segregation of age-0 and age-1+ polar cod (*Boreogadus saida*) over the annual cycle in the Canadian Beaufort Sea Polar. Biol. 39, 1023–1037. https://doi.org/10.1007/s00300-015-1811-z.

Geoffroy, M., Robert, D., Darnis, G., Fortier, L., 2011. The aggregation of polar cod (*Boreogadus saida*) in the deep Atlantic layer of ice-covered Amundsen Gulf (Beaufort Sea) in winter. Polar Biol. 34, 1959–1971. https://doi.org/10.1007/s00300-011-1019-9.

Gjøsæter, H., Ingvaldsen, R., Christiansen, J.S., 2020. Acoustic scattering layers reveal a faunal connection across the Fram Strait. Prog. Oceanogr. 185, 102348. https://doi.org/10.1016/j.pocean.2020.102348.

Gjøsæter, H., Wiebe, P.H., Knutsen, T., Ingvaldsen, R.B., 2017. Evidence of diel vertical Migration of mesopelagic sound-scattering organisms in the Arctic. Front. Mar. Sci. 4, 332. https://doi.org/10.3389/fmars.2017.00332.

Gosselin, M., Levasseur, M., Wheeler, P.A., Horner, R.A., Booth, B.C., 1997. New measurements of phytoplankton and ice algal production in the Arctic Ocean. Deep-Sea Res II 44, 1623–1644. https://doi.org/10.1016/S0967-0645(97)00054-4.

Gradinger, R.R., Bluhm, B.A., 2004. In-situ observations on the distribution and behavior of amphipods and Arctic cod (*Boreogadus saida*) under the sea ice of the High Arctic Canada Basin. Polar Biol. 27, 595–603. https://doi.org/10.1007/s00300-004-0630-4.

Handegard, N.O., Patel, R., Hjellvik, V., 2005. Tracking individual fish from a moving platform using a split-beam transducer. J. Acoust. Soc. Am. 118, 2210–2223. https://doi.org/10.1121/1.2011410.

Hansen, C., Nash, R.D.M., Drinkwater, K.F., Sætre Hjøllo, S., 2019. Management scenarios under climate change – A study of the Nordic and Barents Seas. Front. Mar. Sci. 6, 668. https://doi.org/10.3389/fmars.2019.00668.

Harris, P.T., Macmillan-Lawler, M., Kullerud, L., Rice, J.C., 2018. Arctic marine conservation is not prepared for the coming melt. ICES J. Mar. Sci. 75, 61–71. https://doi.org/10.1093/icesjms/fsx153.

Hauser, D.D.W., Laidre, K.L., Parker-Stetter, S.L., Horne, J.K., Suydam, R.S., Richard, P. R., 2015. Regional diving behavior of Pacific Arctic beluga whales *Delphinapterus leucas* and possible associations with prey. Mar. Ecol. Prog. Ser. 541, 245–264. https://doi.org/10.3354/meps11530.

Hauser, D.D.W., Laidre, K.L., Suydam, R.S., Richard, P.R., 2014. Population-specific home ranges and migration timing of Pacific Arctic beluga whales (*Delphinapterus leucas*). Polar Biol. 37, 1171–1183. https://doi.org/10.1007/s00300-014-1510-1.

Hoag, H., 2017. Nations put science before fishing in the Arctic – Historic fishing ban gives scientists time to probe ecology as northern waters warm. Science 358, 1235. https://doi.org/10.1126/science.358.6368.1235.

Hop, H., Gjøsæter, H., 2013. Polar cod (*Boreogadus saida*) and capelin (*Mallotus villosus*) as key species in marine food webs of the Arctic and the Barents Sea. Mar. Biol. Res. 9, 878–894. https://doi.org/10.1080/17451000.2013.775458.

ICES, 2019a. Barents Sea Ecoregion – Ecosystem overview. In: Report of the ICES Advisory Committee, 2019. ICES Advice 2019, Section 5.1, 12 pp. http://doi.org/10.17895/ices.advice.5747.

ICES, 2019b. Arctic Fisheries Working Group (AFWG). ICES Scientific Reports. 1:30. 934 pp. http://doi.org/10.17895/ices.pub.5292.

IPCC, 2013. Climate Change 2013: The Physical Science Basis. Contribution of Working Group I to the Fifth Assessment Report of the Intergovernmental Panel on Climate Change. Stocker, T.F., et al. (Eds.), Cambridge University Press, Cambridge, United Kingdom and New York, NY, USA, 1535 pp. https://www.ipcc.ch/report/ar5/wg1/.

IPCC, 2018. Global warming of 1.5°C. An IPCC Special Report on the impacts of global warming of 1.5°C above pre-industrial levels and related global greenhouse gas emission pathways, in the context of strengthening the global response to the threat of climate change, sustainable development, and efforts to eradicate poverty. Masson-Delmotte, V., et al. (Eds.), https://www.ipcc.ch/sr15/.

Irigoien, X., Klevjer, T.A., Røstad, A., Martinez, U., Boyra, G., Acuña, J.L., Bode, A., Echevarria, F., Gonzalez-Gordillo, J.I., Hernandez-Leon, S., Agusti, S., Aksnes, D.L., Duarte, C.M., Kaartvedt, S., 2014. Large mesopelagic fishes biomass and trophic efficiency in the open ocean. Nature Comm. 5, 3217. https://doi.org/10.1038/ncomms4271.

Jakobsson, M., et al., 2012. The International Bathymetric Chart of the Arctic Ocean (IBCAO) Version 3.0. Geophys. Res. Lett. 39, L12609. https://doi.org/10.1029/2012GL052219.

Jordan, A.D., Møller, P.R., Nielsen, J.G., 2003. Revision of the Arctic cod genus *Arctogadus*. J. Fish Biol. 62, 1339–1352. https://doi.org/10.1046/j.1095-8649.2003.00115.x.

Kieser, R., Mulligan, T.J., 1983. Analysis of echo counting data: A model. Can. J. Fish. Aquat. Sci. 41, 451–458. https://doi.org/10.1139/f84-054.

Klevjer, T.A., Irigoien, X., Røstad, A., Fraile-Nuez, E., Benítez-Barrios, V.M., Kaartvedt, S., 2016. Large scale patterns in vertical distribution and behaviour of mesopelagic scattering layers. Sci. Rep. 6, 19873. https://doi.org/10.1038/srep19873.

Knudsen, H.P., 2009. Long-term evaluation of scientific-echosounder performance. ICES J. Mar. Sci. 66, 1335–1340. https://doi.org/10.1093/icesjms/fsp025.

Knutsen, T., Hosia, A., Falkenhaug, T., Skern-Mauritzen, R., Wiebe, P.H., Larsen, R.B., Aglen, A., Berg, E., 2018. Coincident mass occurrence of gelatinous zooplankton in northern Norway. Front. Mar. Sci. 5, 158. https://doi.org/10.3389/fmars.2018.00158.

Knutsen, T., Wiebe, P.H., Gjøsæter, H., Ingvaldsen, R.B., Lien, G., 2017. High latitude epipelagic and mesopelagic scattering layers – A reference for future Arctic ecosystem change. Front. Mar. Sci. 4, 334. https://doi.org/10.3389/fmars.2017.00334.

Kobayashi, H.A., 1974. Growth cycle and related vertical distribution of the thecosomatous pteropod *Spiratella* ("*Limacina*") *helicina* in the central Arctic Ocean. Marine Biol. 26, 295–301. https://doi.org/10.1007/BF00391513.

Korneliussen, R.J., 2000. Measurement and removal of echo integration noise. ICES J. Mar. Sci. 57, 1204–1217. https://doi.org/10.1006/jmsc.2000.0806.

Korneliussen, R.J., Heggelund, Y., Macaulay, G.J., Patel, D., Johnsen, E., Eliassen, I.K., 2016. Acoustic identification of marine species using a feature library. Meth. Oceanogr. 17, 187–205. https://doi.org/10.1016/j.mio.2016.09.002.

Korneliussen, R.J., Ona, E., Eliassen, I.K., Heggelund, Y., Patel, R., Godø, O.R., Giertsen, C., Patel, D., Nornes, E., Bekkvik, T., Knudsen, H.P., Lien, G., 2006. The Large-Scale Survey System – LSSS. In: Proceedings of the 29th Scandinavian Symposium on Physical Acoustics (Ustaoset), 6 pp. https://dwoc07ze9j3lr.cloudfront.net/1438757001/p2006_sspa_korneliussen_et_al_lsss.pdf.

Kosobokova, K.N., Hopcroft, R.R., Hirche, H.J., 2011. Patterns of zooplankton diversity through the depths of the Arctic's central basins. Mar. Biodiv. 41, 29–50. https://doi.org/10.1007/s12526-010-0057-9.

Kwok, R., 2018. Arctic sea ice thickness, volume, and multiyear ice coverage: losses and coupled variability (1958–2018). Environ. Res. Lett. 13, 105005. https://doi.org/10.1088/1748-9326/aae3ec.

Laxon, S.W., Giles, K.A., Ridout, A.L., Wingham, D.J., Willatt, R., Cullen, R., Kwok, R., Schweiger, A., Zhang, J., Haas, C., Hendricks, S., Krishfield, R., Kurtz, N., Farrell, S., Davidson, M., 2013. CryoSat-2 estimates of Arctic sea ice thickness and volume. Geophys. Res. Lett. 40, 732–737. https://doi.org/10.1002/grl.50193.

Logerwell, E., et al., 2015. Fish communities across a spectrum of habitats in the western Beaufort Sea and Chukchi Sea. Prog. Oceanogr. 136, 115–132. https://doi.org/10.1016/j.pocean.2015.05.013.

MacLennan, D.N., Fernandes, P.G., Dalen, J., 2002. A consistent approach to definitions and symbols in fisheries acoustics. ICES J. Mar. Sci. 59, 365–369. https://doi.org/10.1006/jmsc.2001.1158.

Mamylov, V.S., 1988. Results of in situ target strength measurements of fisheries objects in the North Atlantic. In: Berdichevsky, Z.M, et al. (Eds.), Instrumental Methods for Stock Size Estimation of Fishable Objects. Manual for scientific work. PINRO, Murmansk. pp. 3–18.

Mapstone, G.M., 2014. Global diversity and review of Siphonophorae (Cnidaria: Hydrozoa). PLoS ONE 9 (2), e87737. https://doi.org/10.1371/journal.pone.0087737.

Margulis, R., 1982. A new siphonophore *Rudjakovia plicata* gen. N., sp. N., (Coelenterata, Hydrozoa) from the Polar Basin and some notes on other siphonophores. Zoologicheskii Zhurnal 61, 440–444.

McWhinnie, S.F., 2009. The tragedy of the commons in international fisheries: An empirical examination. J. Envir. Econom. Managem. 57, 321–333. https://doi.org/10.1016/j.jeem.2008.07.008.

Mecklenburg, C.W., Lynghammar, A., Johannesen, E., Byrkjedal, I., Christiansen, J.S., Dolgov, A.V., Karamushko, O.V., Mecklenburg, T.A., Møller, P.R., Steinke, D., Wienerroither, R.M., 2018. Marine Fishes of the Arctic Region, Volume I. Conservation of Arctic Flora and Fauna, Akureyri, Iceland. https://www.caff.is/monitoring-series/451-marine-fishes-of-the-arctic-region-vol-1.

Melnikov, I.A., Chernova, N.V., 2013. Characteristics of under-ice swarming of polar cod *Boreogadus saida* (Gadidae) in the Central Arctic Ocean. J. Ichthyol. 53, 7–15. https://link.springer.com/article/10.1134%2FS0032945213010086.

Mitson, R.B., Wood, R.J., 1961. An automatic method of counting fish echoes. ICES J. Mar. Sci. 26, 281–291. https://doi.org/10.1093/icesjms/26.3.281.

Mueter, F.J., Nahrgang, J., Nelson, R.J., Berge, J., 2016. The ecology of gadid fishes in the circumpolar Arctic with a special emphasis on the polar cod (*Boreogadus saida*). Polar Biol. 30, 961–967. https://doi.org/10.1007/s00300-016-1965-3.

Nahrgang, J., Varpe, Ø., Korshunova, E., Murzina, S., Hallanger, I.G., Vieweg, I., Berge, J., 2014. Gender specific reproductive strategies of an Arctic key species (*Boreogadus saida*) and implications of climate change. PLoS ONE 6 (5), e98452. https://doi.org/10.1371/journal.pone.0098452.

Nesis, K.N., 1971. The squid [*Gonatus fabricii* (Licht.)] in the center of the Arctic Basin. Hydrobiological J. 7, 76–79.

Nesis, K.N., 2001. West-Arctic and East-Arctic distributional ranges of cephalopods. Sarsia 86, 1–11. https://doi.org/10.1080/00364827.2001.10420456.

Norheim, E., Klevjer, T.A., Aksnes, D.L., 2016. Evidence for light-controlled migration amplitude of a sound scattering layer in the Norwegian Sea. Mar. Ecol. Progr. Ser. 551, 45–52. https://doi.org/10.3354/meps11731.

Olli, K., Wassmann, P., Reigstad, M., Ratkova, T.N., Arashkevich, E., Pasternak, A., Matrai, P.A., Knulst, J., Tranvik, L., Klais, R., Jacobsen, A., 2007. The fate of production in the central Arctic Ocean – top-down regulation by zooplankton expatriates? Progr. Oceanogr. 72, 84–113. https://doi.org/10.1016/j.pocean.2006.08.002.

Ona, E., Hansen, K., 1986. In situ target strength observations of haddock. ICES CM. 1986/B:39, 14 pp. https://imr.brage.unit.no/imr-xmlui/handle/11250/104127.

Ona, E., Mazauric, V., Andersen, L.N., 2009. Calibration methods for two scientific multibeam systems. ICES J. Mar. Sci. 66, 1326–1334. https://doi.org/10.1093/icesjms/fsp125.

Overland, J.E., Wang, M., 2013. When will the summer Arctic be nearly sea ice free? Geophys. Res. Lett. 40, 2097–2101. https://doi.org/10.1002/grl.50316.

PAME, 2013. Large Marine Ecosystems (LMEs) of the Arctic area: Revision of the Arctic LME map 15th of May 2013. 2nd Edition. PAME International Secretariat, Akureyri, Iceland. 19 pp. http://www.research.kobe-u.ac.jp/gsics-pcrc/sympo/20160728/documents/Session4/04PAME_revised_LME_map.pdf.

Pedersen, G., Korneliussen, R.J., 2009. The relative frequency response derived from individually separated targets of northeast Arctic cod (*Gadus morhua*), saithe (*Pollarchius virens*), and Norway pout (*Trisopterus esmarkii*). ICES J Mar. Sci. 66, 1149–1154. https://doi.org/10.1093/icesjms/fsp070.

Proud, R., Handegard, N.O., Kloser, R.J., Cox, M.J., Brierly, A.S., 2018. From siphonophores to deep scattering layers: uncertainty ranges for the estimation of global mesopelagic fish biomass. ICES J. Mar. Sci. 76, 718–733. https://doi.org/10.1093/icesjms/fsy037.

Raskoff, K.A., Hopcroft, R.R., Kosobokova, K.N., Purcell, J.E., Youngbluth, M., 2010. Jellies under ice: ROV observations from the Arctic 2005 hidden ocean expedition. Deep-Sea Res. II 57, 111–126. https://doi.org/10.1016/j.dsr2.2009.08.010.

Reeves, R.R., 1998. Distribution, abundance and biology of ringed seals (*Phoca hispida*): an overview. NAMMCO Sci. Publ. 1, 9–45. https://doi.org/10.7557/3.2979.

Renner, A.H.H., Sundfjord, A., Janout, M.A., Ingvaldsen, R.B., Beszczynska-Möller, A., Pickart, R.S., Pérez-Hernández, M.D., 2018. Variability and redistribution of heat in the Atlantic water boundary current north of Svalbard. JGR Oceans. https://doi.org/10.1029/2018JC013814.

Rudels, B., 2015. Arctic Ocean circulation, processes and water masses: A description of observations and ideas with focus on the period prior to the International Polar Year 2007–2009. Prog. Oceanogr. 132, 22–67. https://doi.org/10.1016/j.pocean.2013.11.006.

Rudels, B., 2019. Arctic Ocean Circulation. Encyclopedia of Ocean Sciences (2nd Edition), edited by John H. Steele, J.H. (Ed.), Academic Press, 2009, pp. 211–225. https://www.sciencedirect.com/science/article/pii/B9780123744739006019.

Sameoto, D., Wiebe, P., Runge, J., Postel, L., Dunn, J., Miller, C., Coombs, S., 2000. Collecting zooplankton. In: Harris, R., Wiebe, P., Lenz, J., Skjoldal, H.R., Huntley, M. (Eds.), ICES Zooplankton Methodology Manual. Academic Press, New York, pp. 55–81.

Schauer, U., Rudels, B., Jones, E.P., Anderson, L.G., Muench, R.D., Björk, G., Swift, J.H., Ivanov, V., Larsson, A.M., 2002. Confluence and redistribution of Atlantic water in the Nansen, Amundsen and Makarov basins. Ann. Geophys. 20, 257–273. https://doi.org/10.5194/angeo-20-257-2002.

Screen, J.A., Williamson, D., 2017. Ice-free Arctic at 1.5 °C? Nat. Clim. Change 7, 230–231. https://www.nature.com/articles/nclimate3248.

Siegelman-Charbit, L., Planque, B., 2016. Abundant mesopelagic fauna at oceanic high latitudes. Mar. Ecol. Prog. Ser. 546, 277–282. https://doi.org/10.3354/meps11661.

Simmonds, J., MacLennan, D., 2005. Fisheries Acoustics: Theory and Practice, 2nd ed. Blackwell Science, Oxford, p. 437 pp..

Simrad, 2018. Simrad EK80 reference manual, release 1.11.x. https://www.simrad.com.

Snoeijs-Leijonmalm, P., Flores, H., Volckaert, F., Niehoff, B., Schaafsma, F.L., Hjelm J, Hentati-Sundberg J., Niiranen, S., Crépin, A.S., Österblom, H., 2020. Review of the research knowledge and gaps on fish populations, fisheries and linked ecosystems in the Central Arctic Ocean (CAO). Report, European Commission, 80 pp. https://op.europa.eu/en/publication-detail/-/publication/aae1e59e-46fe-11ea-b81b-01aa75ed71a1/language-en.

Spall, M.A., 2019. Dynamics and thermodynamics of the mean transpolar drift and ice thickness in the Arctic Ocean. J. Climate 32, 8449–8463. https://doi.org/10.1175/JCLI-D-19-0252.1.

Stranne, C., Mayer, L., Jakobsson, M., Weidner, E., Jerram, K., Weber, T.C., Anderson, L. G., Nilsson, J., Björk, G., Gårdfeldt, K., 2018. Acoustic mapping of mixed layer depth. Ocean Sci. 14, 503–514. https://doi.org/10.5194/os-14-503-2018.

Stranne, C., Mayer, L., Weber, T.C., Ruddick, B.R., Jakobsson, M., Jerram, K., Weidner, E., Nilsson, J., Gårdfeldt, K., 2017. Acoustic mapping of thermohaline staircases in the Arctic Ocean. Sci. Rep. 7, 15192. https://www.nature.com/articles/s41598-017-15486-3.

UNCLOS, 1982. United Nations Convention on the Law of the Sea. https://www.un.org/depts/los/convention_agreements/convention_overview_convention.htm.

Vacquié-Garcia, J., Lydersen, C., Marques, T.A., Aars, J., Ahonen, H., Skern-Mauritzen, M., Øien, N., Kovacs, K.M., 2017. Late summer distribution and abundance of ice-associated whales in the Norwegian High Arctic. Endang. Spec. Res. 32, 59–70. https://doi.org/10.3354/esr00791.

van der Meeren, G.I., Prozorkevich, D., (Eds.), 2019. Survey report from the joint Norwegian/Russian Ecosystem Survey in the Barents Sea and adjacent waters, August-October 2018. IMR/PINRO Joint Report Series 2019/2, 1–93. https://www.hi.no/en/hi/nettrapporter/imrpinro/2019/survey-report-from-the-joint-norwegian-russian-ecosystem-survey-in-the-barents-sea-and-adjacent-waters-august-october-2018-nr.-2-2019.

van Meurs, R., Splettstoesser, J.F., 2003. Farthest north polar bear (*Ursus maritimus*). Arctic 56, 309. http://doi.org/10.14430/arctic626.

Van Pelt, T.I., Huntington, H.P., Romanenko, O.V., Mueter, F.J., 2017. The missing middle: Central Arctic Ocean gaps in fishery research and science coordination. Mar. Policy 85, 79–86. https://doi.org/10.1016/j.marpol.2017.08.008.

Von Duyke, A.L., Douglas, D.C., Herreman, J.K., Crawford, J.A., 2019. Ringed seal (Pusa hispida) seasonal movements, diving, and haul-out behavior in the Beaufort, Chukchi, and Bering Seas (2011-2017). Ecol. Evol. http://doi.org/10.1002/ece3.6302.

Young, R.E., 1973. Evidence for spawning by *Gonatus* sp. (Cephalopoda: Teuthoidea) in the High Arctic Ocean. Nautilus 87, 53–58.